

POLARIS UNDERGROUND PROJECT AT SNO (P.U.P.S)

Report on Year 1 Studies

NWMO TR-2007-16

December 2007

Gail Atkinson and San Linn Kaka
Carleton University

nwmo

NUCLEAR WASTE
MANAGEMENT
ORGANIZATION

SOCIÉTÉ DE GESTION
DES DÉCHETS
NUCLÉAIRES



Nuclear Waste Management Organization
22 St. Clair Avenue East, 6th Floor
Toronto, Ontario
M4T 2S3
Canada

Tel: 416-934-9814
Web: www.nwmo.ca

**POLARIS UNDERGROUND PROJECT AT SNO (P.U.P.S.)
Report on Year 1 Studies**

NWMO TR-2007-16

December 2007

Gail Atkinson and SanLinn Kaka
Carleton University

Disclaimer:

This report does not necessarily reflect the views or position of the Nuclear Waste Management Organization, its directors, officers, employees and agents (the "NWMO") and unless otherwise specifically stated, is made available to the public by the NWMO for information only. The contents of this report reflect the views of the author(s) who are solely responsible for the text and its conclusions as well as the accuracy of any data used in its creation. The NWMO does not make any warranty, express or implied, or assume any legal liability or responsibility for the accuracy, completeness, or usefulness of any information disclosed, or represent that the use of any information would not infringe privately owned rights. Any reference to a specific commercial product, process or service by trade name, trademark, manufacturer, or otherwise, does not constitute or imply its endorsement, recommendation, or preference by NWMO.

ABSTRACT

Title: POLARIS UNDERGROUND PROJECT AT SNO (P.U.P.S.)
Year 1 Report
Report No.: NWMO TR-2007-16
Author(s): Gail Atkinson and SanLinn Kaka
Company: Carleton University
Date: December, 2007

Abstract

This report describes Year 1 studies of the PUPS (POLARIS Underground Project at Sudbury Neutrino Observatory) project. The main objective of PUPS is to conduct an experiment in 3-dimensional seismic monitoring at Sudbury Neutrino Observatory (SNO) to address a range of scientific or engineering objectives related to underground tunnel operations. In the first year, useable signals from about 15 local and regional events were recorded and analyzed, including near-source signals from the MN 4.1 Lively earthquake. The influence of near-surface site effects for rock sites and the potential effects of seismic response due to the free surface in cavities and tunnels was studied. Comparisons of the signals measured on the surface to those at subsurface locations were carried out to address these effects. A number of important ground-motion parameters, such as the high-frequency decay parameter, κ , and earthquake stress drop, were also evaluated for local and regional events.

A key conclusion is that underground motions appear to be lower than those at the surface, but there is much inter-event variability, and a larger number of recordings is required to firmly establish mean trends. The ratio of horizontal to vertical component motions on the surface is larger than that underground. For underground sites, horizontal and vertical component amplitudes are similar. There is significant high-frequency decay of ground motions from nearby events at both surface and underground sites, suggesting an important source-related high-frequency decay (“ κ ”) effect. Stress drops from small local earthquakes, of magnitude 1.4 to 2.8, are generally low (<50 bars). These factors (κ and low stress) may act to limit high-frequency ground motions.

Further monitoring and analysis is recommended to better define the trends noted in the 1st year of study. Additional areas of investigation are also proposed to take advantage of the unique geometry of this experiment.

TABLE OF CONTENTS

	<u>Page</u>
ABSTRACT	v
1. INTRODUCTION	1
2. DATA ANALYSIS	4
2.1 DETAILS OF STATION GEOMETRY	4
2.2 DATA PROCESSING	6
2.3 EXAMPLE TIME SERIES AND SPECTRA.....	8
3. THE LIVELY EARTHQUAKE	12
4. COMPARISON OF MOTIONS ON SURFACE TO UNDERGROUND	13
4.1 PROBLEM BACKGROUND	13
4.2 ANALYSIS OF FOURIER SPECTRA	14
4.3 ANALYSIS OF RESPONSE SPECTRA.....	20
5. HIGH-FREQUENCY DECAY PARAMETER, KAPPA.....	26
6. IMPLICATIONS OF GROUND MOTIONS FOR STRESS DROP	30
7. CONCLUSIONS AND FUTURE WORK	31
7.1 CONCLUSIONS	31
7.2 FUTURE WORK	31
ACKNOWLEDGEMENTS	33
REFERENCES	33
Appendix 1 - THE LIVELY EARTHQUAKE SEQUENCE.....	35

LIST OF TABLES

	<u>Page</u>
Table 1: Analyzed Events (Event #> 100 are teleseismic, at >1000 km).....	6

LIST OF FIGURES

	<u>Page</u>
Figure 1: Cross-section of SNOlab location. Surface facilities are located near the head of Shaft #9. Horizontal distance from #9 shaft to SNO is about 1 km.....	1
Figure 2: Location of PUPS seismograph stations.....	2
Figure 3: Seismic events near SNO Aug. 2006-May 2007.....	3
Figure 4: Plan of SNO Underground Monitoring Sites.....	5
Figure 5: Validation of sacprocessT program used to compute Fourier spectra. Black line shows FFT of sac_ascii data at SUNO (vertical component of velocity), divided by instrument broadband gain factor. Blue line shows inferred acceleration spectrum in cm/s ² . Red crosses are smoothed spectral acceleration values from program “agram” for the same signal.....	8
Figure 6: Corrected accelerograms (cm/s ²) at 2 underground stations for Event 6 (MN 1.4 at 4 km). Note time scale is arbitrary at 46SNO (no GPS time).....	9
Figure 7: Noise Fourier acceleration spectrum for a 30-sec window.....	10
Figure 8: Fourier acceleration spectra for Event 15 (M2.5 at 10 km). Stn1=SSNO, 2=11SNO, 3=46SNO, 4=LSNO, 5=DSNO. Stations 1, 2 are on the surface.....	11
Figure 9: Response spectra for Event 15, showing 3 components for underground stations 46SNO (3=blue) and LSNO (4=red) and surface station 11SNO (2=gray).....	12
Figure 10: 3-component mean log spectral ratios with respect to underground Station 3 (46SNO): Fourier spectra.....	15
Figure 11: 3-component mean log spectral ratios with respect to underground Station 4 (LSNO): Fourier spectra.....	16
Figure 12: 3-component mean log spectral ratios with respect to underground Station 5 (DSNO): Fourier spectra.....	17
Figure 13: Mean log ratios of surface stations to underground stations: 3-component average of Fourier spectra.....	18
Figure 14: Mean log ratios of surface stations to underground stations: Vertical component of Fourier spectra.....	19
Figure 15: Mean log ratios of surface stations to underground stations: Horizontal component of Fourier spectra.....	20
Figure 16: Response spectra (5% damped peak spectral acceleration) for Event 14 (M 2.1 at 10 km). Black triangles show the average (calculated by averaging log spectra over all components at all stations) response spectrum.....	21
Figure 17: Ratio of response spectra to event average, for horizontal (H) components and vertical (V) components on the surface and underground.....	22
Figure 18: Log ratios for response spectra at surface Station 1 (SSNO) relative to event averages, for horizontal (H) and vertical (V) components.....	23
Figure 19: Log ratios for response spectra at surface Station 2 (11SNO) relative to event averages, for horizontal (H) and vertical (V) components.....	24

Figure 20: Log ratios for response spectra at underground Station 3 (46SNO) relative to event averages, for horizontal (H) and vertical (V) components.....	24
Figure 21: Log ratios for response spectra at underground Station 4 (LSNO) relative to event averages, for horizontal (H) and vertical (V).....	25
Figure 22: Log ratios for response spectra at surface Station 5 (DSNO) relative to event averages, for horizontal (H) and vertical (V) components.....	25
Figure 23: Typical behaviour of Fourier displacement spectra for small local earthquakes for vertical (top) and horizontal (bottom) components: Station 3 (46SNO).....	28
Figure 24: Average high-frequency decay (3-10) Hz for surface and underground stations, on vertical (top) and horizontal (bottom) components.....	29
Figure 25: Correlation between MN (Nuttli magnitude) and preliminary estimates of M (moment magnitude).....	30

1. INTRODUCTION

The PUPS project takes advantage of the unique 3-dimensional geometry offered by the SNO lab, located at a depth of 2 km beneath the Inco Creighton Mine in Sudbury, Ontario, and its access tunnels through Shaft #9. Figure 1 shows a cross-section of the mine, with the location of the SNO lab indicated. There are also surface facilities, including a major laboratory building for SNO, at the surface near the head of Shaft #9.

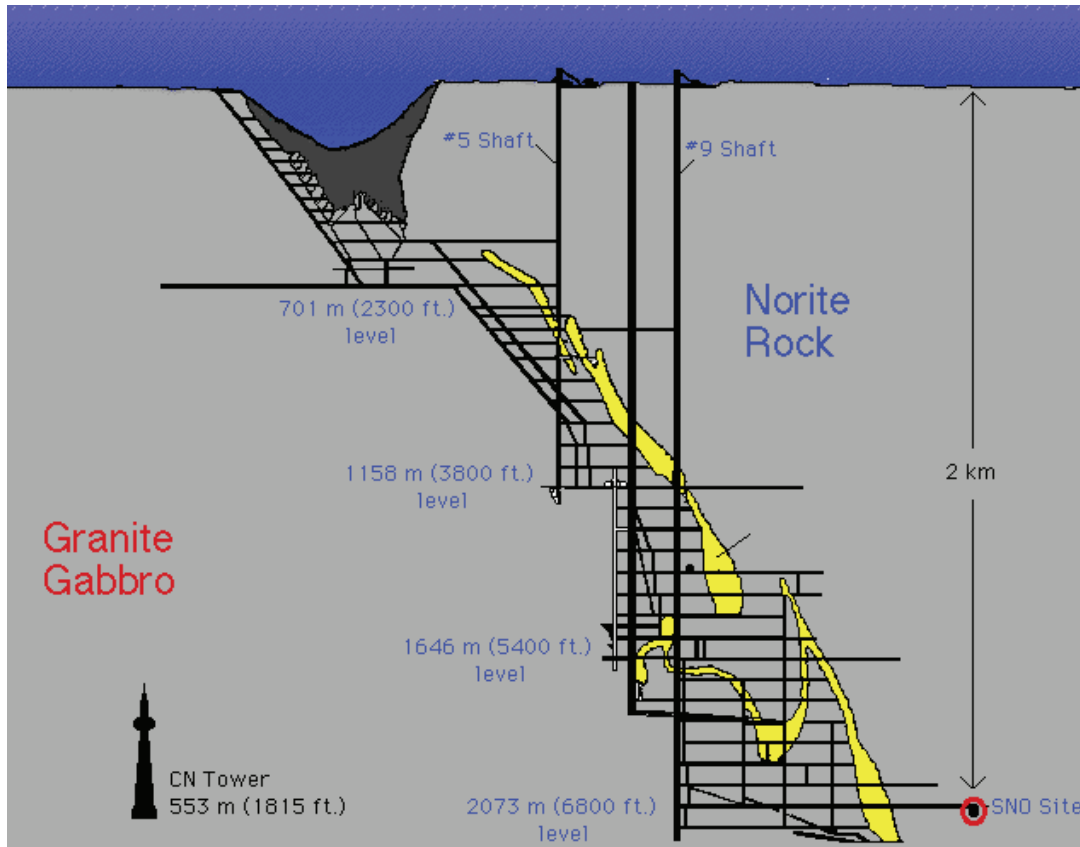


Figure 1: Cross-section of SNOlab location. Surface facilities are located near the head of Shaft #9. Horizontal distance from #9 shaft to SNO is about 1 km

Five portable Taurus seismograph units obtained from the POLARIS Consortium, each with 3-component broadband seismometers sampling at 200 samples/sec, have been installed in the following locations:

1. Station SSNO (=station 1) - A short distance from the SNO Lab building on the surface. This location has power and internet access.
2. Station 11SNO (=station 2) - On the surface, near shaft #11.
3. Station 46SNO (=station 3) - At the 4600 m level, within the SNO satellite lab.

4. Station LSNO (=station 4) - At the SNO level (2073 m), at a location along the drift between the lab and shaft #9.
5. Station DSNO (=station 5) - Within the SNO lab at 2 km depth (2073 m). This is a modern lab facility, with on-site power and internet access.

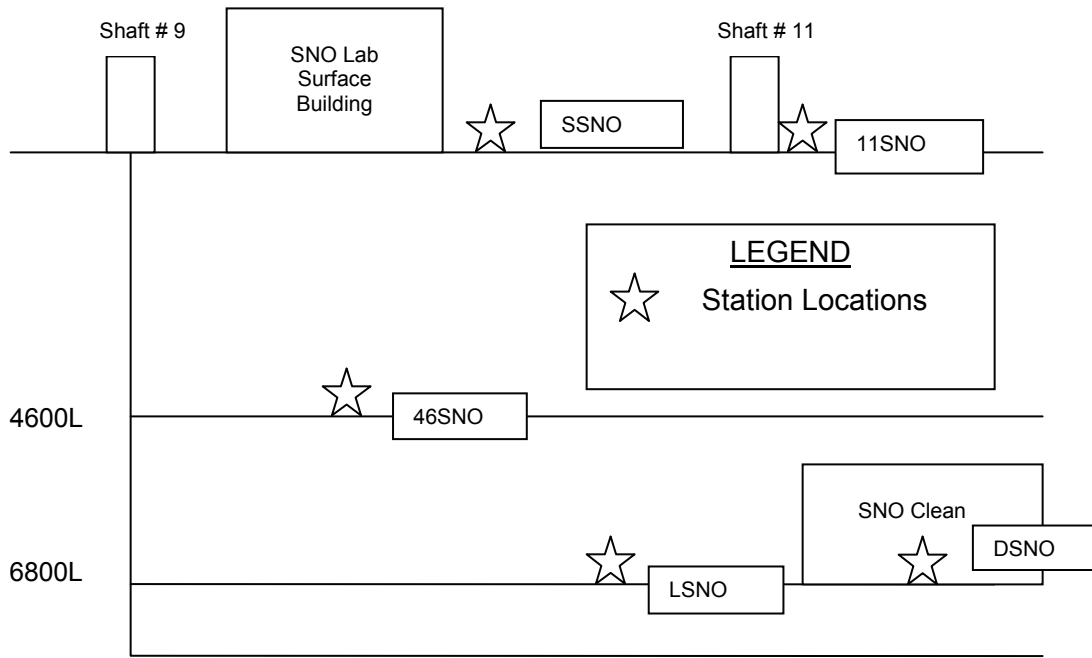


Figure 2: Location of PUPS seismograph stations

The installations were made possible through the cooperation of the SNO Lab and Inco. Figure 2 shows the station locations. Stations DSNO and SSNO have power and internet access. The other sites (LSNO, 46SNO and 11SNO) are stand-alone, using internal and battery power, with internal clock. The sites are within or on hard rock. All 5 stations are currently operating and collecting data (as of September, 2007); data collection began in August, 2006.

The focus of this study is engineering seismology studies related to source and site effects, particularly on how ground-motion amplitudes at deep underground sites are related to the corresponding motions for sites on the surface. This is a critical issue for the evaluation of seismic response on deep geologic repository and other underground facilities. SNO was selected for this study because of its deep underground facility. Figure 3 shows the seismic events recorded near SNO that are included in this report; they cover the time period from August 2006 - May 2007 (events post-May 2007 have not yet been processed and analyzed).

As part of this study, the signals of all events recorded at both underground and surface levels as shown on Figure 3 are processed and analysed. Signal processing involves the transformation of recorded signals from time domain to the frequency domain, the removal of

instrument response to obtain absolute ground-motion amplitudes, and the analysis of signal to noise to determine the appropriate frequency range for analysis for each event, at each station. The focus of this study is on the frequency domain representation of site effects, and ground-motion results obtained from the Lively earthquake sequence (events of M 3 to 4+ on Figure 3).

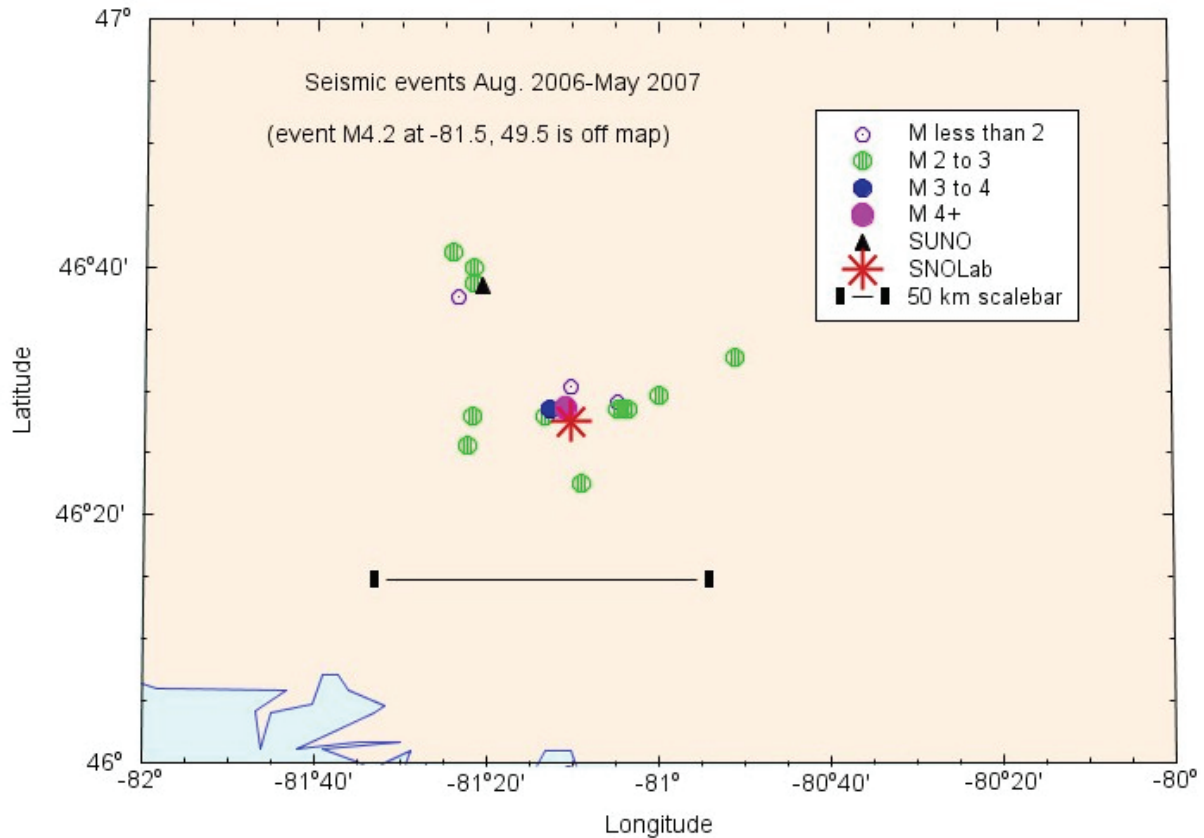


Figure 3: Seismic events near SNO Aug. 2006-May 2007

The project objectives involve investigations in 3 topic areas relevant to the understanding of ground motions in underground tunnels and caverns. These topic areas are as follows:

1. *Near-surface site effects for rock sites:* Most seismographic stations in eastern Canada are located on hard rock sites with conditions similar to those at Sudbury. It is important to understand the extent to which such signals are influenced by near-surface site effects, in order to properly interpret observed earthquake ground motions. By comparing signals observed on the surface at SNO to those at subsurface locations, empirical models of rock site response may be developed and evaluated in terms of gross rock properties. Understanding how ground motions are amplified by the near-surface materials is a critical topic for analyzing the seismic hazard to underground waste storage facilities, and for the safety of underground engineered operations.
2. *Investigation of the free surface effect in cavities and tunnels:* Theoretically, when a seismic wave encounters a free surface, the amplitude of ground motion doubles. This

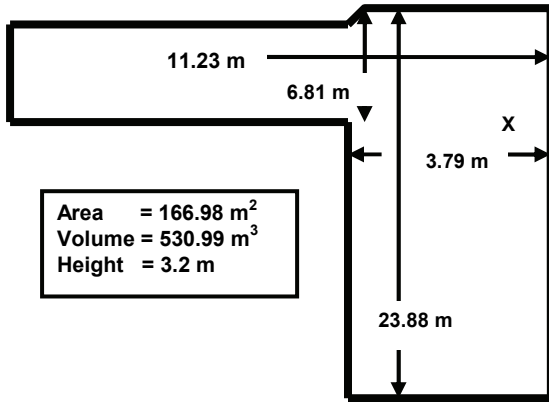
is referred to as the “free surface effect”. Do the sensors in cavities and tunnels, which are located way below the surface, experience the same free-surface effect? Are the observed free-surface effects the same for all frequencies, or does the size of tunnel or cavity play an important role? It may be that the free surface effect scales as a function of size of cavity and the wavelength of each harmonic. This project provides an opportunity to experimentally investigate the real values of free surface effects at different depth in tunnels or cavities. Like topic 1, this is an important issue for seismic hazards to underground facilities.

3. *Lively earthquake sequence*: A mining-induced earthquake of MN4.1 at a depth of 2.35 km, at Lively, Ontario, near Sudbury, offers a rare close-up view of a moderate event in an intraplate setting. It was recorded by the 5 three-component broadband PUPS seismographic stations at hypocentral distances from 0.4 to 3 km, as well as by regional seismographs at distances from 22 to hundreds of km. The close proximity of this station to the event enabled detection of abundant small aftershocks (70 during the first 12 hours) and recording of rarely-seen near-field components of the seismic wavefield. The fortuitous occurrence of this highly significant event, so close to the instruments, could not have been foreseen when the project was initiated. We made some adjustments in the program study areas to take advantage of this unique event. We analyze local and regional recordings of the Lively event to characterize and provide a preliminary interpretation of near-source ground motions in a cavern from a moderate, nearby seismic event.

2. DATA ANALYSIS

2.1 DETAILS OF STATION GEOMETRY

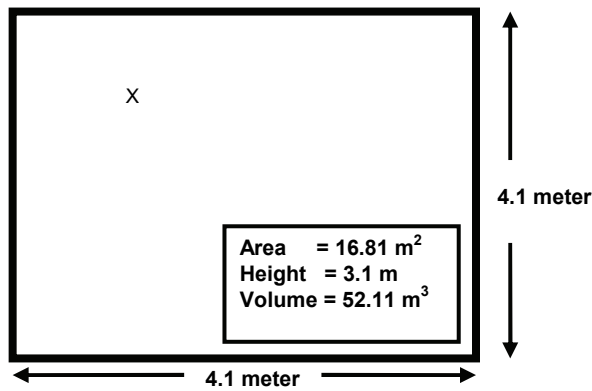
The dimensions of the underground openings at all monitoring sites were measured, so that any systematic differences between ground-motion amplitudes at different stations may potentially be correlated with cavity size. These measurements are presented in Figure 4.



DSNO:

Seismic monitoring station located at the 6800ft level within the SNO lab
latitude 460 28' 30'' N and longitude 810 12' 04'' W

X = Seismometer (21 cm in diameter)

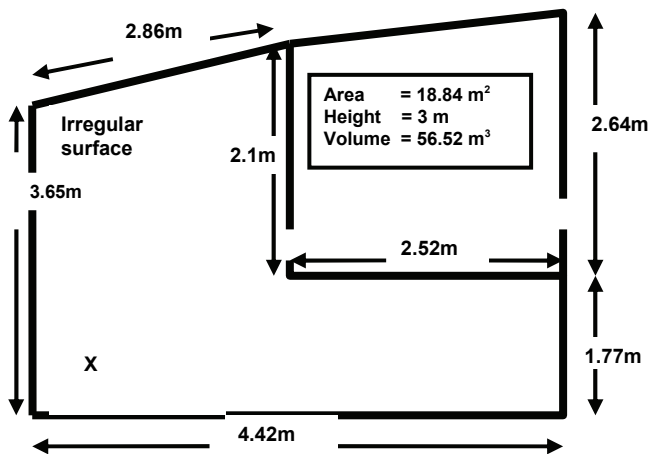


LSNO:

Seismic monitoring station located in the latrine
(along the drift between the SNO lab and shaft #9)

latitude 460 28' 13.9'' N and longitude 810 12' 32.6'' W

X = Seismometer (21 cm in diameter)



46SNO:

Seismic monitoring station located at the 4600ft level, within the SNO satellite lab

latitude 460 25' 27.92'' N and longitude 810 10' 18.44'' W

X = Seismometer (21 cm in diameter)

Figure 4: Plan of SNO Underground Monitoring Sites

2.2 DATA PROCESSING

All processed signals at both underground and surface levels that were recorded between August 2006 and May 2007 are listed in Table 1. This includes 25 local and regional earthquakes, and several teleseismic events. For the teleseismic events, only preliminary analyses were possible within the scope of the Year 1 work. Further teleseismic analyses, using additional signals, are planned for Year 2.

The local and regional events provide a good picture of motions at intermediate to high frequencies, while the teleseismic events may be able to provide some constraints at long periods (<1 Hz). Local-event magnitudes ranged from 1.4 to 4.1 MN. During this monitoring period, the data from the MN4.1 earthquake near Lively, Ontario on Nov. 29, 2006, was also recorded and is described detailed in Section 3.

Table 1: Analyzed Events (Event #> 100 are teleseismic, at >1000 km). (blank fields for some events indicate events of unknown magnitude and location; these would be very small events not well-recorded by the GSC network)

Event No.	Year	month	Day	MN	Latitude	Longitude	Epicentral distance (km)
1	2006	8	24				
2	2006	8	24	2.8	46.47	-81.36	12
3	2006	9	1	2.2	46.65	-81.36	22
4	2006	9	4	2.0	46.50	-82.56	104
5	2006	9	17	2.4	46.48	-81.06	11
6	2006	9	18	1.4	46.51	-81.17	4
7	2006	11	29	4.1	46.48	-81.18	<1
8	2006	11	29	2.0	46.47	-81.22	<1
9	2006	11	29	3.1	46.48	-81.21	<1
10	2006	12	7	4.2	49.51	-81.53	338
11	2006	12	21				
12	2006	12	21	2.4	46.50	-81.00	15
13	2006	12	31	2.1	46.48	-81.08	9
14	2007	1	2	2.1	46.48	-81.07	10
15	2007	1	2	2.5	46.48	-81.07	10
16	2007	1	2	2.2	46.38	-81.15	12
17	2007	1	7	2.0	46.67	-81.36	24
18	2007	1	11	1.9	46.49	-81.08	9
19	2007	1	24	2.3	46.55	-80.85	28
20	2007	1	26	1.8	46.63	-81.39	22
21	2007	3	2	2.8	48.25	-78.44	286
22	2007	3	2				
23	2007	3	9	2.8	46.43	-81.37	14
24	2007	3	9				
25	2007	5	13	2.8	46.69	-81.40	28
100	2006	11	13	6.8	-26.04	-63.24	>1000
101	2006	11	15	8.3	46.60	153.23	>1000
102	2006	12	26	7.1	21.83	120.54	>1000
103	2007	1	13	8.1	46.27	154.46	>1000
104	2007	1	21	7.5	1.22	126.40	>1000
105	2007	4	1	8.1	-8.48	156.98	>1000

Data processing involves the transformation of recorded signals to the frequency domain, removal of instrument response to obtain absolute ground-motion amplitudes, and the analysis of signal to noise to determine the appropriate frequency range for analysis for each event, at each station. The focus here is on the frequency domain representation of site effects. The transformation of recorded signals for all events was performed using a FORTRAN program “sacprocessT” written specifically to expedite the processing. We begin by windowing the shear-wave portions of the recorded signals. Recorded data are in a “miniseed” (Standard for Exchange of Earthquake Data) format which is first converted to sac-ascii format. Conversion was done by a publicly available program called HAM. More information on the HAM program can be found at seismological software library at the Observatories and Research Facilities for European Seismology (ORFEUS) <http://www.orfeus-eu.org/links/softwarelib.htm>. The sac_ascii data are given in velocity counts, uncorrected for instrument response. The “sacprocessT” program does some filtering, including Butterworth filtering and removal of any long-period trends or offsets. It computes the Fourier spectrum by Fast Fourier Transform (FFT) and removes the instrument response for the Trillium seismometers that recorded the signals, by dividing the spectrum by the constant broadband gain level of the instrument, and adjusting for the shape of the Trillium response at high frequencies. It also outputs response spectra and corrected accelerograms. We have validated the Fourier spectrum obtained by the “sacprocessT” program by comparing it to the smoothed spectrum obtained from another program, “agram”, which works with data recorded in the GSC GSE format. Figure 5 shows this validation exercise. It plots the Fourier velocity transform of the SUNO spectrum divided by the constant broadband gain level for the instrument (from sacprocessT), as well as the inferred Fourier acceleration spectrum converted to units of cm/s^2 . The acceleration spectrum matches the smoothed result from the “agram” output for SUNO. The “agram” program has been in use for many years and has been used to form the databases for many ground-motion publications (eg. Atkinson and Boore, 1995, 2006; Atkinson, 2004).

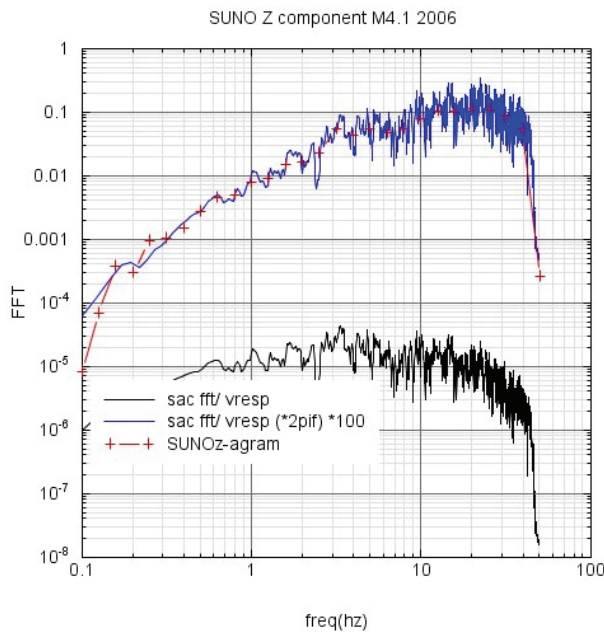


Figure 5: Validation of sacprocessT program used to compute Fourier spectra. Black line shows FFT of sac_ascii data at SUNO (vertical component of velocity), divided by instrument broadband gain factor. Blue line shows inferred acceleration spectrum in cm/s². Red crosses are smoothed spectral acceleration values from program “agram” for the same signal.

2.3 EXAMPLE SPECTRA AND TIME SERIES

All records listed in Table 1 were processed to obtain instrument-corrected time series, Fourier spectra, and response spectra. Figure 6 shows typical corrected accelerograms for a small local earthquake (Event 6, MN1.4 at 4 km). It is apparent that the signal is clear above the noise levels. A more detailed picture of typical noise (as recorded on the day of the Lively earthquake) can be obtained by looking at the spectrum of a noise window over a short period of time (30s). Figure 7 shows the Fourier acceleration spectrum of a noise window; note that noise tends to be relatively high on underground station LSNO (this is near a latrine half-way between the SNO lab and the elevator shaft, and may be a sub-optimal location from a noise point of view), and also on the surface stations, in comparison to 46SNO and DSNO, which are the quietest sites. There is quite a lot of high-frequency noise in this window. On the time history traces, the corrected noise acceleration amplitudes are about 0.003 cm/s² at DSNO in the time interval before the event begins, and an order of magnitude higher (eg. 0.03 cm/s²) on the surface. This noise is most likely caused by mining operations, such as machinery or equipment operating nearby. The noise levels vary with time at each location. Further study of these noise characteristics and their time variability will be made in the 2nd year of the research program. It may be advisable to move stations that are in relatively noisy locations, if quieter locations can be found. It is not possible to eliminate the noise altogether, due to the nature of the facility, but it may be possible to find locations that are quiet a greater proportion of the time.

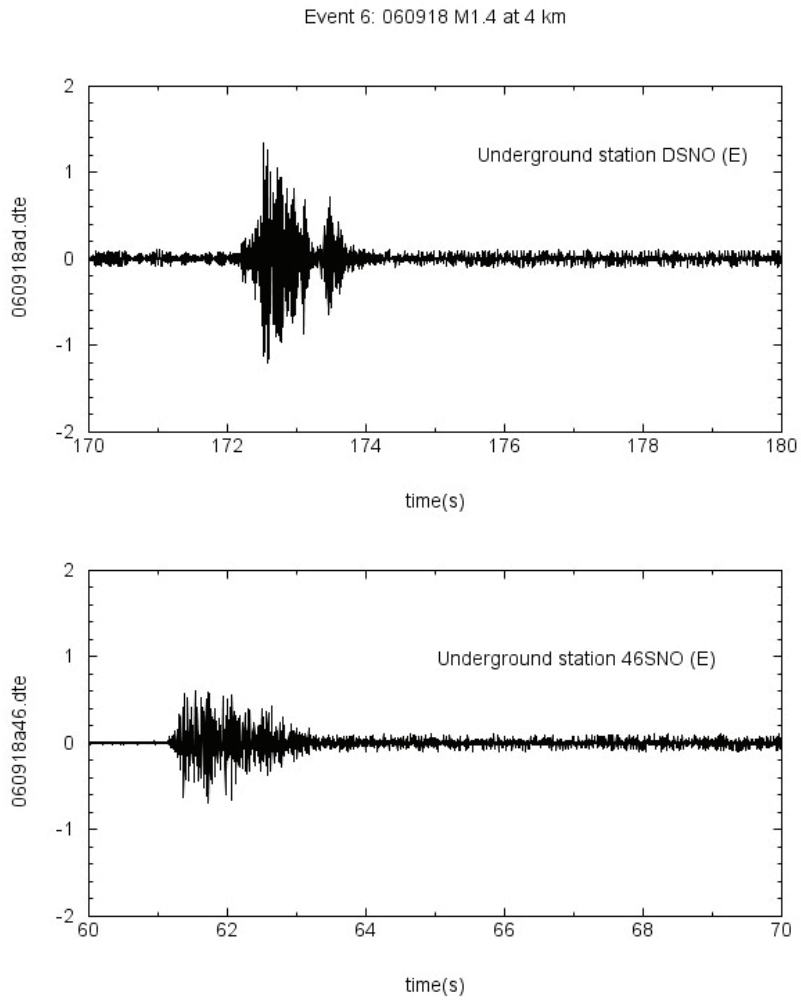


Figure 6: Corrected accelerograms (cm/s²) at 2 underground stations for Event 6 (MN 1.4 at 4 km). Note time scale is arbitrary at 46SNO (no GPS time).

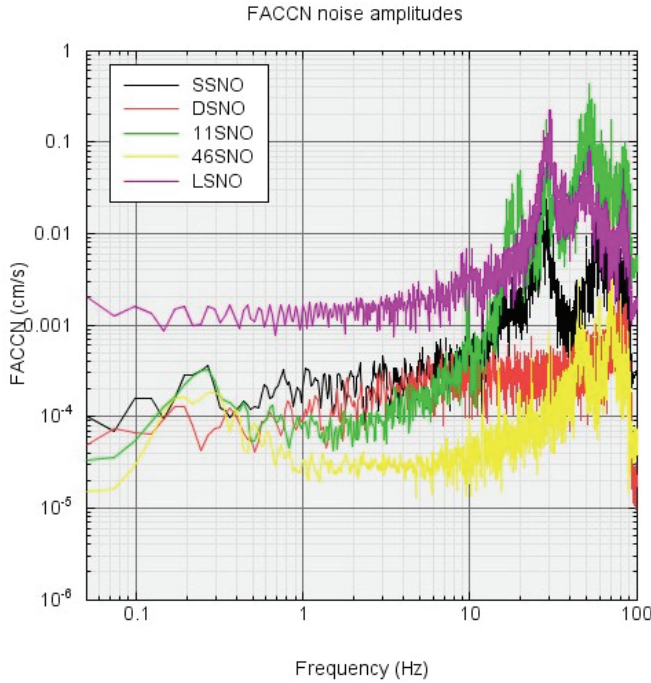


Figure 7: Noise Fourier acceleration spectrum for a 30-sec window.

Figure 8 shows average Fourier acceleration spectra (using a 3-component average for each station) for a typical small local event. Figure 9 plots the corresponding response spectra, in this case showing spectra separately for each component. In Figure 9, the 2 horizontal components are denoted by the last letter e or n, while the vertical component is denoted by the letter z. The letters e and n nominally stand for east and north, but in this case the actual positioning is not known – they are simply two random orthogonal horizontal components. Note that spectra are broadly similar for the different stations (for both Fourier spectra and response spectra). The overall pattern is stable, but a clear trend of amplitudes for one station versus another is not seen in an individual example. To see such trends requires more detailed analysis, as reported in Section 4. Note also that not all stations are available for many events, due to noise and other problems.

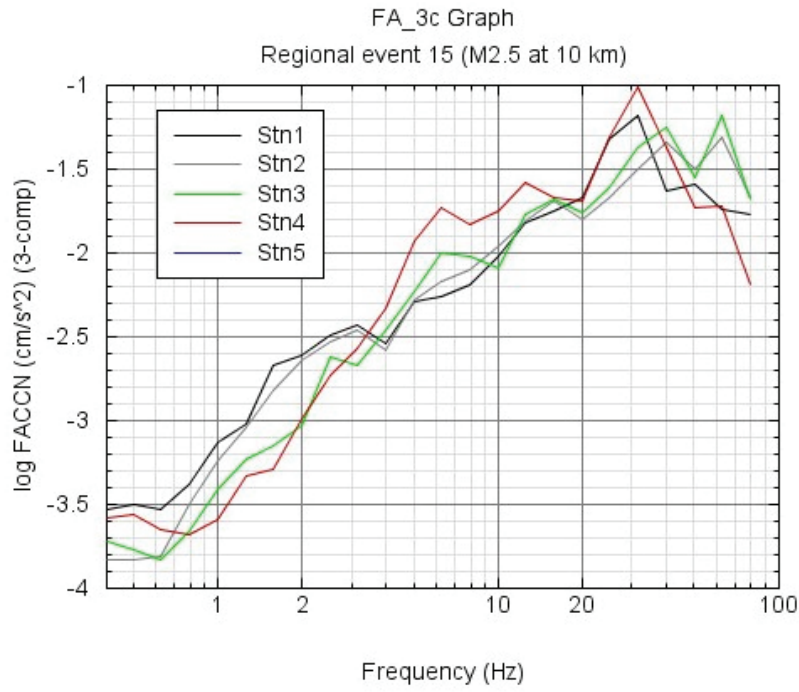


Figure 8: Fourier acceleration spectra for Event 15 (M2.5 at 10 km). Stn1=SSNO, 2=11SNO, 3=46SNO, 4=LSNO, 5=DSNO. Stations 1, 2 are on the surface.

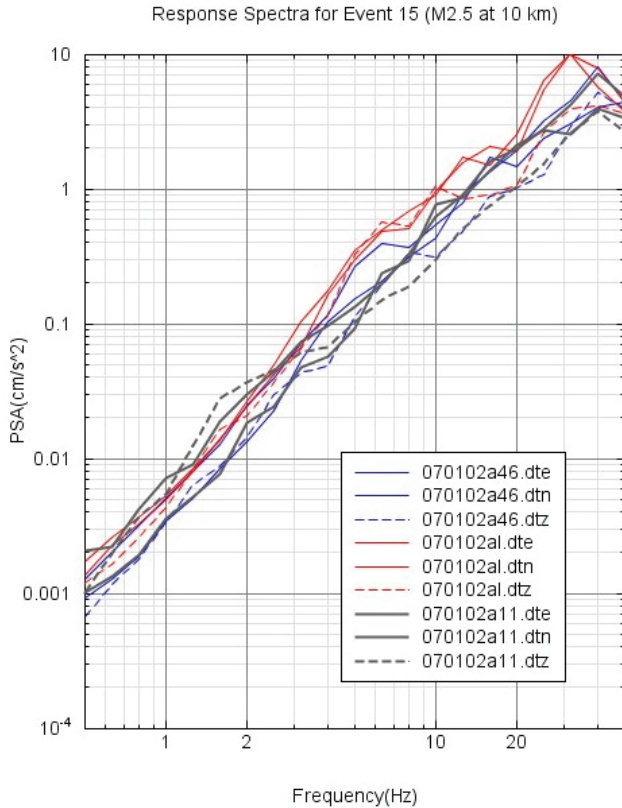


Figure 9: Response spectra for Event 15, showing 3 components for underground stations 46SNO (3=blue) and LSNO (4=red) and surface station 11SNO (2=gray).

3. THE LIVELY EARTHQUAKE SEQUENCE

A shallow moderate earthquake of MN4.1 occurred near Sudbury, Ontario, at 07:22:55 UTC (02:22:55 local time) on Nov. 29, 2006. The event was located 6 km from Lively, Ontario, and was induced by mining activity at INCO's Creighton mine. INCO's in-mine monitoring system, and their subsequent visual inspection, places the event at 46.47 N 81.20 W, at a depth of 2.35 km. This event offers us a rare close-up view of a moderate earthquake, because it was recorded at close distances by the five 3-component broadband PUPS seismographic stations that are installed above and within the Creighton mine. The closest station to the event is within the Sudbury Neutrino Observatory (SNO) lab, which is 2 km beneath the surface, and about 300 m above the event. The event caused no damage to the SNO lab, and only minor damage to the mine workings; there were no injuries. The event was widely felt in the Sudbury, Ontario region, as expected based on instrumental ShakeMaps (www.shakemap.carleton.ca) and confirmed by internet intensity reports (www.earthquakecanada.ca). The mainshock was followed by two significant aftershocks at 2:36 (MN 2.0) and 2:38 (MN 3.1) local time, and by many smaller aftershocks. In addition to the near-source records, this event was well-recorded regionally at distances from 20 km to hundreds of km, by the seismographic stations of the Canadian National Seismographic Network (CNSN) and (POLARIS). As part of this year's studies, we took advantage of this unexpected event to provide a preliminary examination of the recorded ground motions, and

discuss their implications for our understanding of source and attenuation properties in eastern North America (ENA). This work is reported in Appendix 1, as it resulted in a collaborative paper with scientists from the Geological Survey of Canada (this paper is pre-printed as Appendix 1).

Key findings of the study of the Lively earthquake sequence were that the mainshock had a moment magnitude of 3.7 to 3.8 and a Brune stress drop near 20 bars. Recorded ground motions agree with the values predicted by regional ground-motion equations for an event of this magnitude and stress drop, over epicentral distances ranging from 0 to hundreds of km. Subsurface ground-motions, recorded at distances from 0.4 to 1 km above the hypocenter, were a factor of 3 to 10 lower than the apparent source spectra (defined at a reference distance of 1 km) as obtained from hard-rock recordings made on the surface.

4. COMPARISON OF MOTIONS ON SURFACE TO UNDERGROUND

4.1 Problem Background

A key objective of this study is to determine how ground motions recorded in underground cavities compare with those on the Earth's surface. All existing ground-motion prediction equations that are applied in seismic hazard analyses apply to sites on the Earth's surface. Thus in extending seismic hazard analyses and ground-motion estimates to sites underground, the relationship between motions underground and those on the surface is a critical point.

Theoretically, ground-motion amplitudes within the Earth should be lower than those on the surface by a factor of two, due to the "free surface" effect. This refers to the fact that conservation of energy requires amplification by a factor of two in seismic wave amplitudes, when waves traveling through the Earth encounter a free surface. However, instruments underground are not an integral part of a whole Earth, but rather are positioned within cavities. In the case of the PUPS project, these cavities are quite large. One might expect in this case that the waves would not "see" the cavity at long periods (wavelengths much larger than the dimension of the cavity), but that the cavity would act as a free surface at high frequencies (wavelengths much smaller than the cavity dimension).

An additional factor that may moderate underground amplitudes is the higher shear-wave velocity and more competent condition of the bedrock. It is known that near-surface weathering and jointing tends to reduce near-surface shear-wave velocities, even for hard rock sites such as those in Sudbury. For example, typical ENA hard rock sites have surface velocities in the range of 2.8 to 3 km/s, while velocities at a depth of a few km are about 3.5 km/s (Beresnev and Atkinson, 1997). This near-surface gradient acts to amplify seismic waves, with the amplification being an increasing function of frequency (Boore and Joyner, 1997). On the other hand, the increased cracking and weathering near the surface disrupts high-frequency motions and leads to greater energy absorption. There is thus an offsetting factor to the amplification by the velocity gradient, which is typically modeled by the high-frequency decay parameter, kappa (Anderson and Hough, 1984), which is discussed in the next section. The interplay between these two factors could, in general, lead to either smaller or larger motions being recorded underground.

The data being recorded by the PUPS project offer a unique opportunity to gather empirical evidence to document the differences between underground and surficial motions. Most of the signals recorded to date (Table 1) are at a great enough distance from SNO (10 km or more) that the distance from the event to all stations is essentially equal (with the Lively earthquake sequence being a notable exception). Furthermore, due to the nature of high-frequency ground

motions (incoherent signals), directional effects are not significant – path effects are essentially the same for all azimuths. Since the source effects and path effects are the same at all PUPS stations that record the events, any differences in observed ground motions can be attributed to the site conditions of the stations, in particular whether they are on the surface or underground.

To investigate these effects we have analyzed the ratios of surficial stations to those underground in several ways. We describe results obtained from analyses of both the Fourier and response spectra. Response spectra are useful in that they provide a smoother more engineering-focused representation of the ground motions, and they can be compared directly to predictions of ground-motion prediction equations (such as Atkinson and Boore, 2006, for example).

4.2 Analysis of Fourier Spectra

To evaluate the differences in motions at the PUPS stations, we first examine the ratio of the Fourier spectrum at each station to that at every other station that recorded the same event. This provides the amplification at one station relative to another. In this exercise, we use the 3-component average of the Fourier acceleration spectra for each record (where a geometric mean is calculated, by averaging log spectra). There are typically about a dozen such ratios for each station, as events are often not well recorded on all stations (local noise from mine activities often eliminates one or more records). These ratios show much variability from one event to another, indicating that the relationship has a significant stochastic element, and cannot be robustly determined from a small number of recordings. The noise at some stations may also complicate the interpretation of the ratios, as it contributes to the scatter in results.

In Figures 10 to 12, we display the average 3-component ratios to each of the three underground stations, with respect to all other stations; these typically represent averages from 7 to 17 events, depending on the station combination and frequency plotted. The standard deviations of these ratios are also shown. Differences in behaviour between the underground stations are apparent. Station 3 (46SNO) has systematically lower amplitudes than station 1 (SSNO) on the surface, by about 0.2 to 0.3 log units (the ratio of Station 1 to 3 is about 0.2 units on Figure 10); this is nearly a factor of 2. However, the amplitudes at station 3 are similar to those at station 2 (11SNO) on the surface. They tend to be lower than the amplitudes at underground station 4 (LSNO), and higher than those at station 5 (DSNO) at high frequencies. This may be reflecting noise characteristics of the various stations to some extent. Underground stations 3 and 5 are generally quiet, while station 4 tends to be noisier. The standard deviations of the ratios are large, in the range from 0.3 to 0.6 log units, corresponding to factors of two to four.

The ratios for other stations reveal the same trends overall. Ratios to station 4 (LSNO) (Figure 11) tend to be low, meaning the amplitudes at LSNO are high. Ratios to station 5 (DSNO) are high (Figure 12), and dramatically so at high frequencies. This suggests that there may be a high-frequency de-amplification of motions at the DSNO site, possibly because the instrument is within the SNO clean lab. The SNO clean lab is founded on fill. Every effort was made to place the instrument at the edge of the lab, off the fill. However, these ratios suggest that the placement of DSNO may be sub-optimal as a hard-rock underground site. In the longer term, DSNO will be re-sited in the new clean lab facility that is currently being constructed by SNO; SNO is endeavouring to provide a true rock footing for this installation.

The information on the ratios of motions at the surface to those underground, based on the Fourier spectra of regional events, is summarized in Figures 13-15. Figure 13 plots the average ratio of surface stations (using both 11SNO and SSNO) to the 3 underground stations, based on the 3-component record average. Figures 14 and 15 show the same ratios, considering just the vertical component, or horizontal components, respectively. Differences between surface and underground stations appear to be greater for horizontal components than for vertical components; vertical motions underground are similar to those on the surface, while horizontal motions appear to be de-amplified underground, at least on some stations. Overall, some underground stations have lower amplitudes than the surface stations, but LSNO does not, possibly due to noise. The trends are ambiguous.

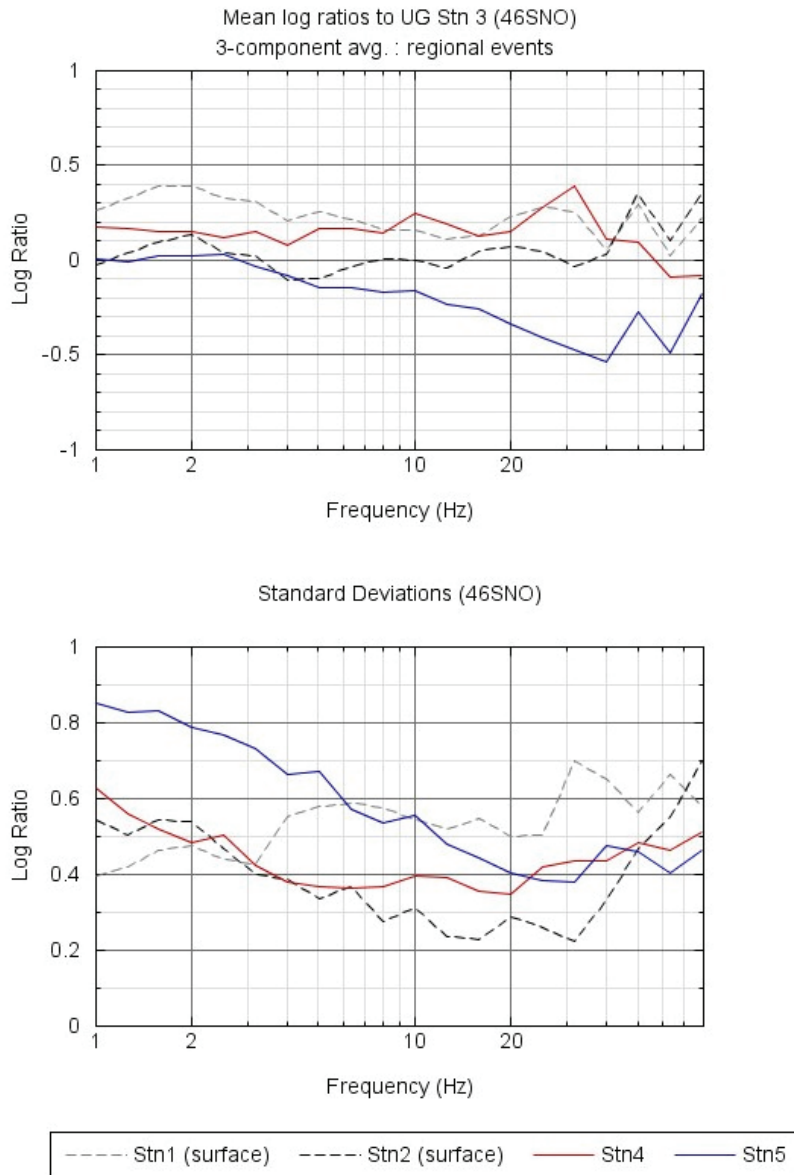


Figure 10: 3-component mean log spectral ratios with respect to underground Station 3 (46SNO): Fourier spectra.

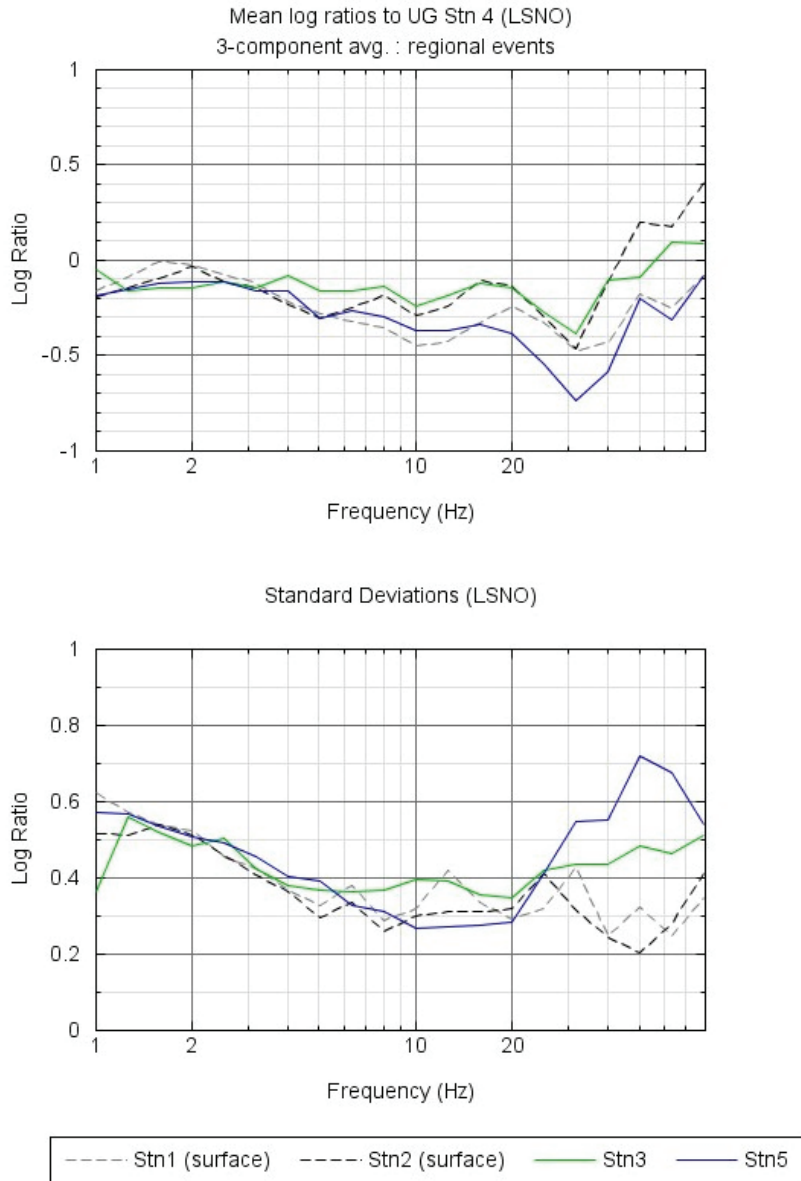


Figure 11: 3-component mean log spectral ratios with respect to underground Station 4 (LSNO): Fourier spectra.

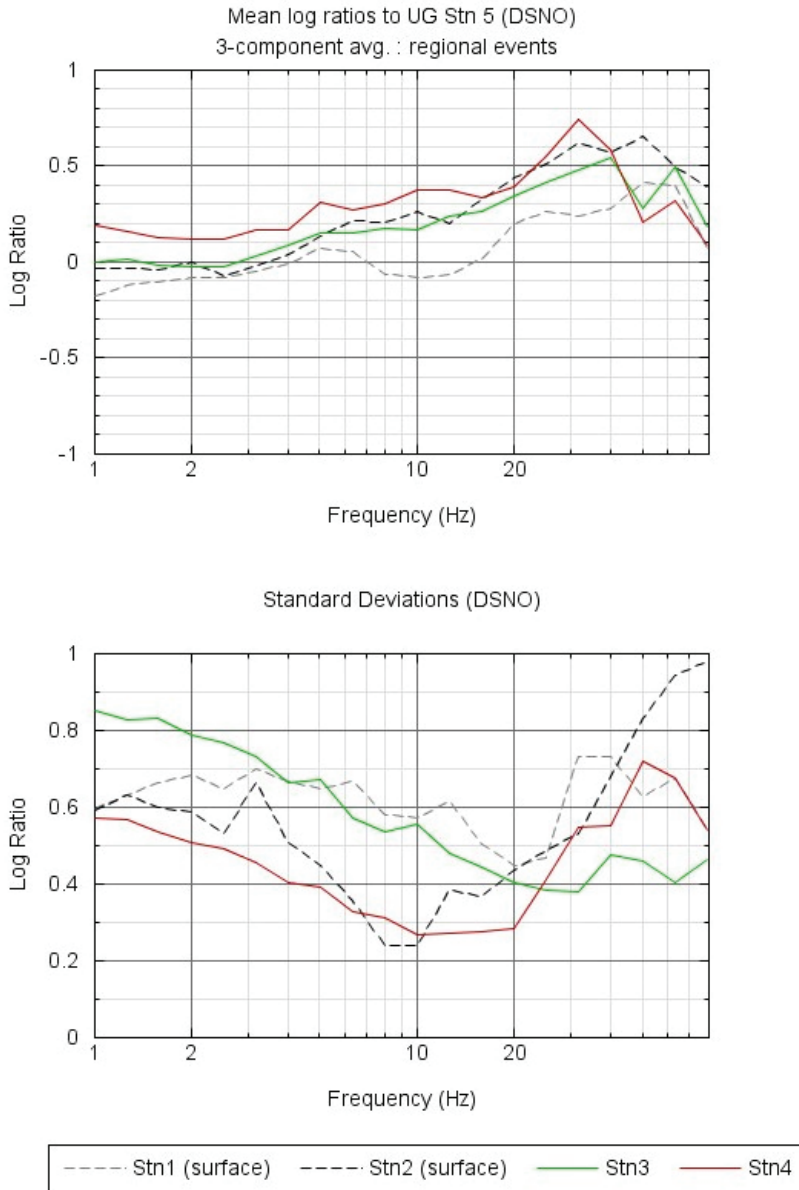


Figure 12: 3-component mean log spectral ratios with respect to underground Station 5 (DSNO): Fourier spectra.

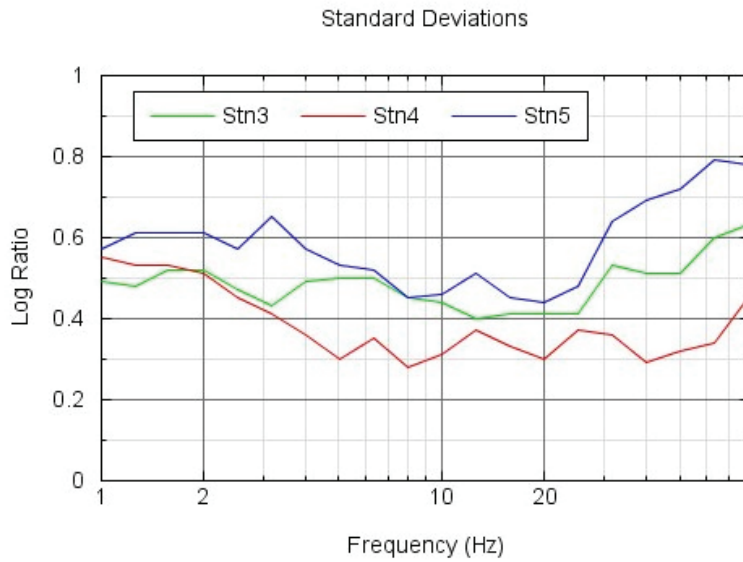
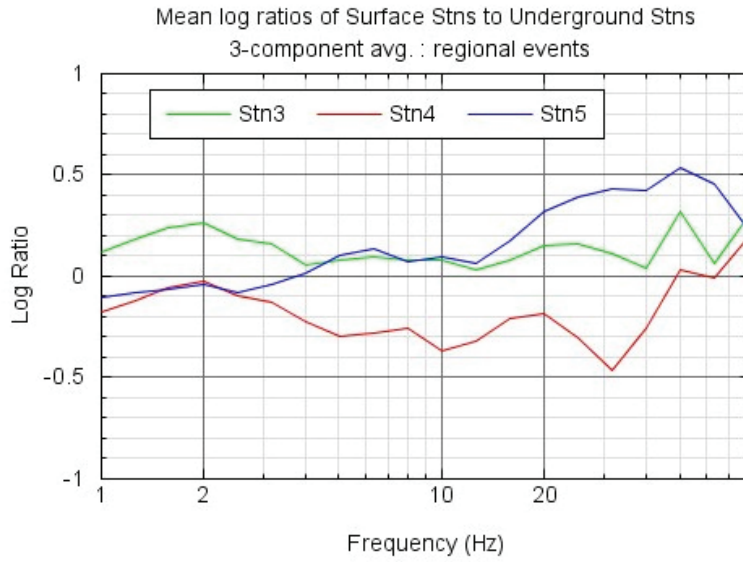


Figure 13: Mean log ratios of surface stations to underground stations: 3-component average of Fourier spectra.

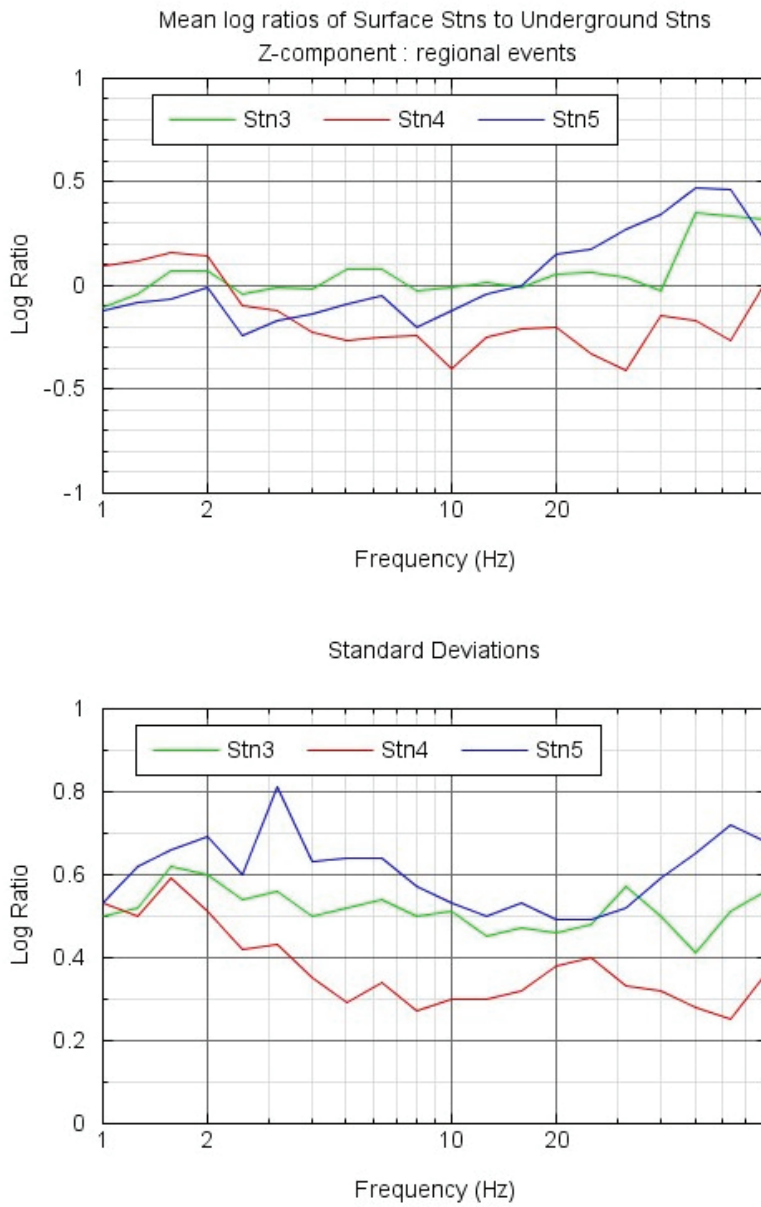


Figure 14: Mean log ratios of surface stations to underground stations: Vertical component of Fourier spectra.

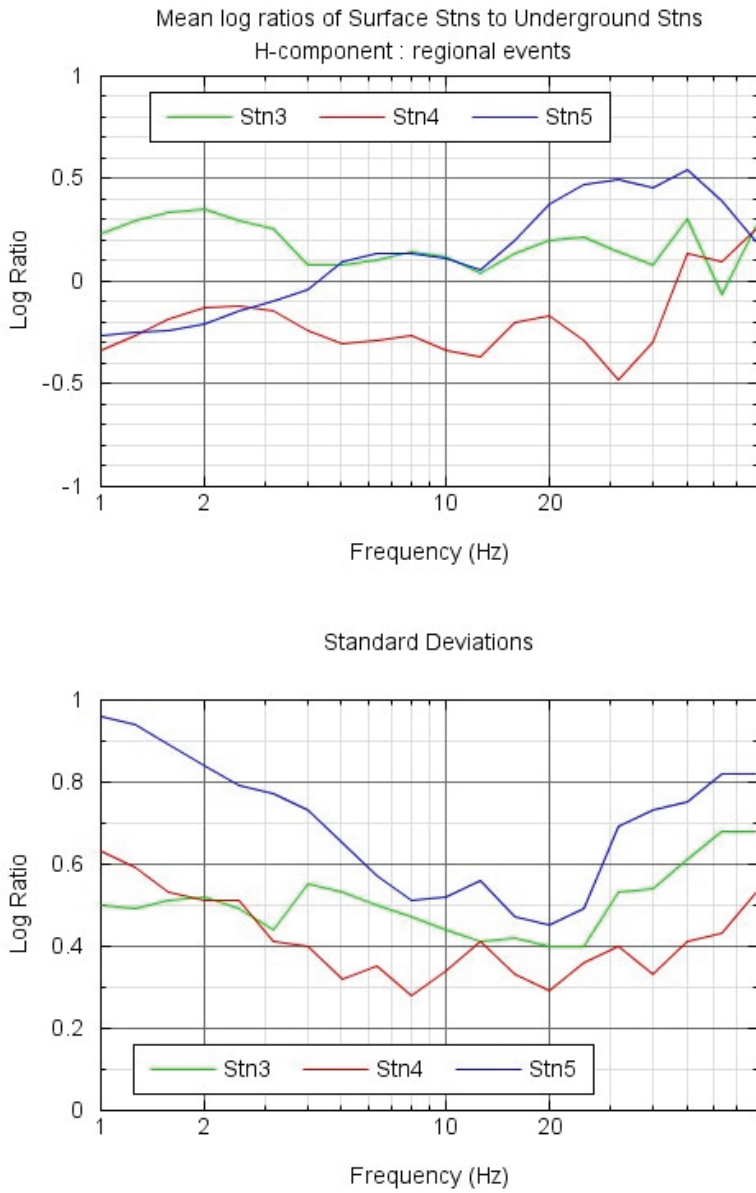


Figure 15: Mean log ratios of surface stations to underground stations: Horizontal component of Fourier spectra.

4.3 Analysis of Response Spectra

The response spectra offer another means of addressing the relative behaviour of underground versus surface stations. They may offer some advantages in comparison to Fourier spectra, in that response spectra have a smoother behaviour with frequency, and are less influenced by noise, as they reflect the peak response of an oscillator to the signal, rather than being a cumulative measure. We therefore also use response spectra (5% damped pseudo-

acceleration) to examine this issue. (Note: 5% damping is used because it is the standard reference value for ground-motion prediction equations.)

In this analysis, we examine the behaviour of each station relative to the average response spectrum for the event. As illustrated in Figure 16 for an event of MN2.1 at 10 km, the response spectra are well behaved, and a computed average of all recorded components is a good measure of the overall spectrum for that event.

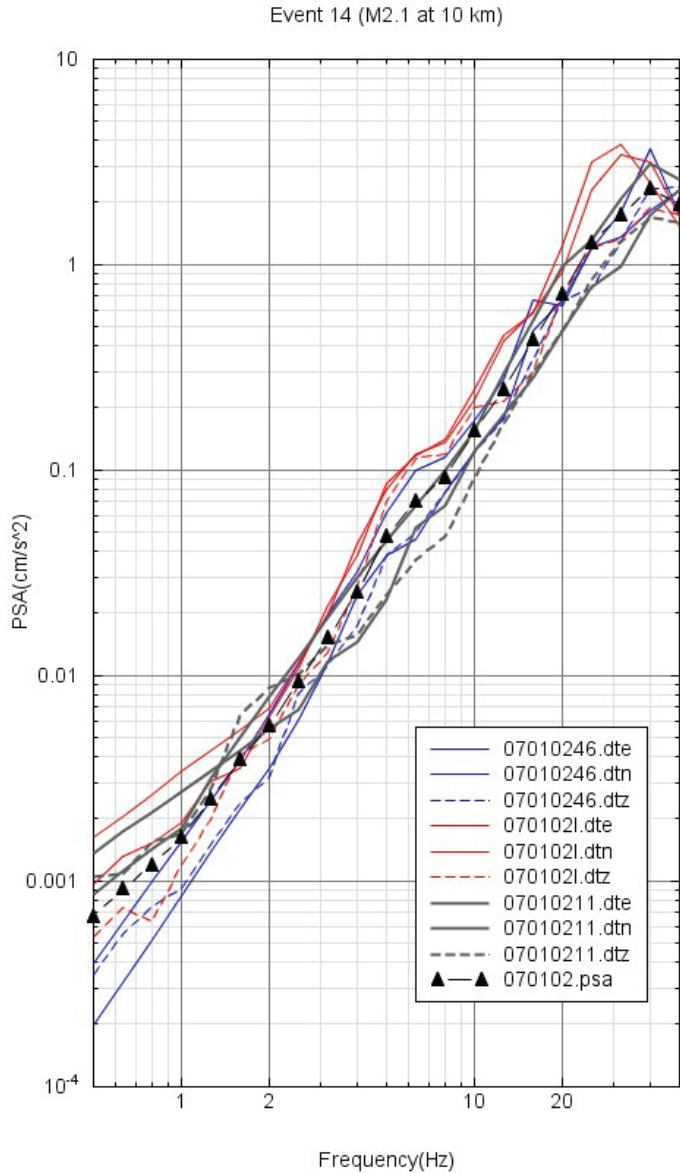


Figure 16: Response spectra (5% damped peak spectral acceleration) for Event 14 (M 2.1 at 10 km). Black triangles show the average (calculated by averaging log spectra over all components at all stations) response spectrum.

We first examine the relative behaviour of horizontal versus vertical components of ground motion, as horizontal motions are more amplified on the surface than are vertical components, due to the velocity gradient effect (Siddiqi and Atkinson, 2002). We would not necessarily expect the same to be the case 2 km underground, as there will be minimal gradient effect. Examination of the ratios of response spectra to their event averages does indeed suggest a difference in behaviour underground. This is shown on Figure 17, which plots the average ratio of horizontal and vertical components to the corresponding “event average”. The event average is obtained over all stations, both surficial and underground; it provides a reference level for each event against which individual records can be compared. These component ratios are shown as an average for all surface stations, and all underground stations. For the surface stations, there is a clear separation between the horizontal and vertical components, with the horizontals being greater than average (by about a factor of 1.2) and the verticals being correspondingly less than average (by a multiplicative factor of 0.8). For the underground stations, there is only a separation between horizontal and vertical components at high frequencies, above 10 Hz. This suggests that the gradient effect that acts to amplify horizontal components is not present at the underground sites, where the 3 components are approximately equal on average, except possibly at high frequencies.

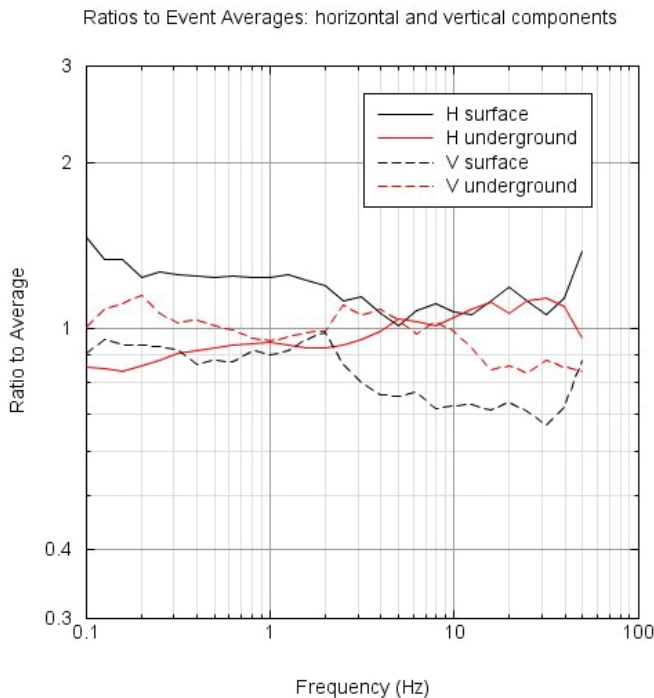


Figure 17: Ratio of response spectra to event average, for horizontal (H) components and vertical (V) components on the surface and underground.

On Figures 18-22 the ratios for each station, with respect to the event averages (where again the event average is taken over all stations), are shown for both horizontal and vertical components. Error bars, plotted just for the horizontal component, show the standard deviation of these ratios. (Error bars are not plotted for the vertical component for clarity purposes, but are of similar magnitude to those for the horizontal component.) Note that the ratio in these

plots is shown in log units, so that a value of 0.3 corresponds to amplification by a factor of two relative to the average, for example.

Overall, the surface stations have response spectra that are above the average on the horizontal components, with SSNO having above-average amplitudes at $f > 1$ Hz, and 11SNO having above-average amplitudes at $f < 1$ Hz. There is a clear separation of horizontal from vertical components, especially at 11SNO where it is about 0.2 log units (a factor of 1.6). This suggests there may be a significant amplification effect on this station. A shear-wave velocity study would be useful to see if there is an explanation for this result in the surficial rock properties.

The underground station 46SNO, which is an excellent, quiet site, shows a relative de-amplification on the horizontal component at lower frequencies. Underground station LSNO, a noisy site, shows an amplification of both horizontal and vertical components by about 0.1 units (factor of 1.3). Underground station DSNO shows a clear deamplification of both horizontal and vertical components, by about 0.2 units (factor of 1.6). Bear in mind that all of these amplifications are just relative (with respect to averages over all stations), and that the variability from one event to another, as reflected by the standard deviation, is large ($>$ factor of 2).

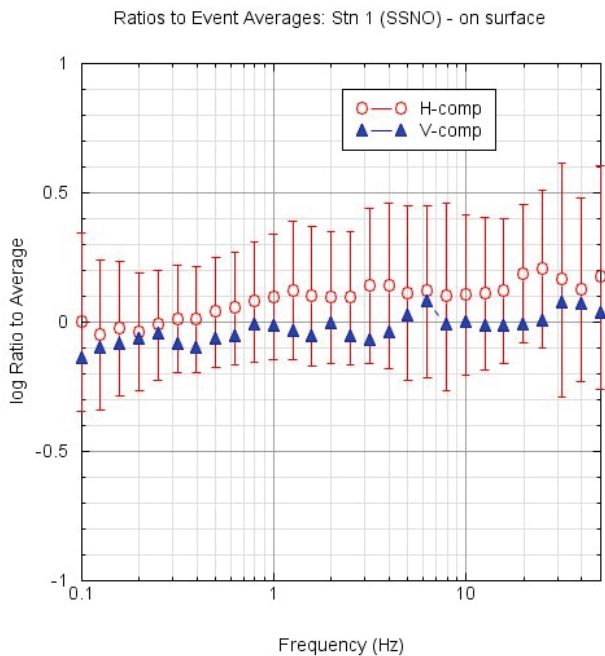


Figure 18: Log ratios for response spectra at surface Station 1 (SSNO) relative to event averages, for horizontal (H) and vertical (V) components.

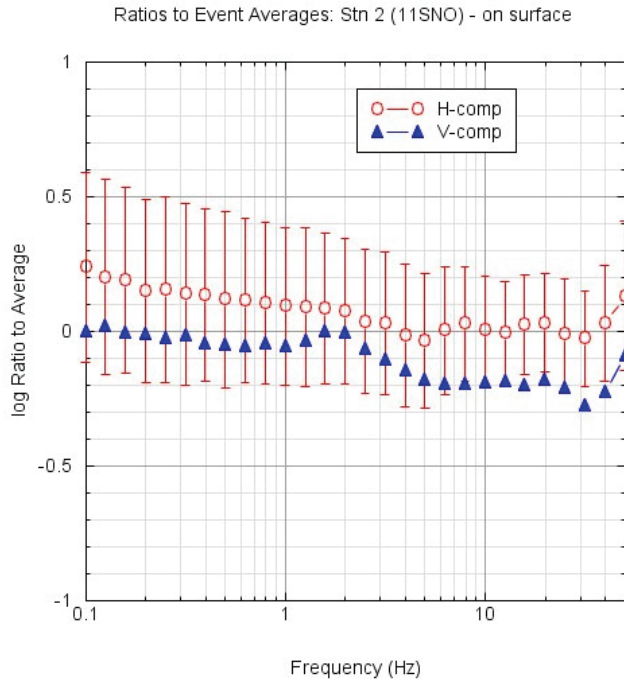


Figure 19: Log ratios for response spectra at surface Station 2 (11SNO) relative to event averages, for horizontal (H) and vertical (V) components.

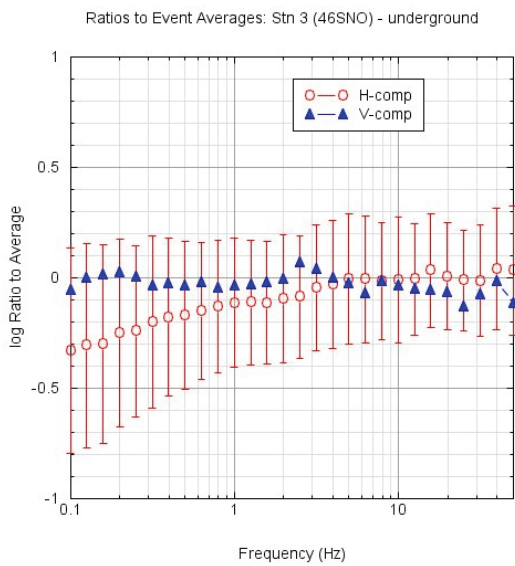


Figure 20: Log ratios for response spectra at underground Station 3 (46SNO) relative to event averages, for horizontal (H) and vertical (V) components.

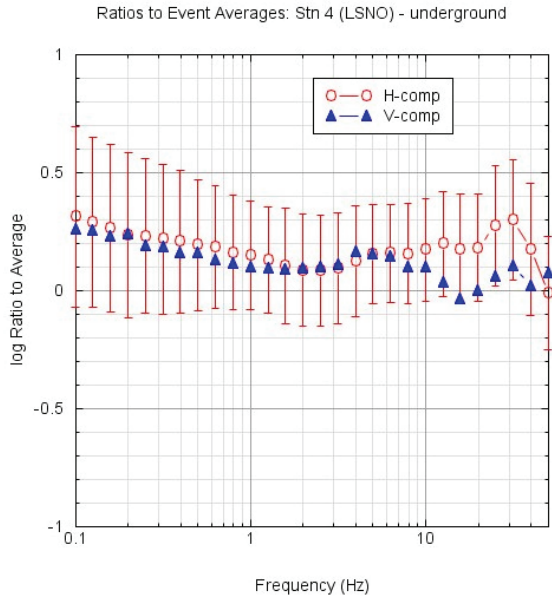


Figure 21: Log ratios for response spectra at underground Station 4 (LSNO) relative to event averages, for horizontal (H) and vertical (V)

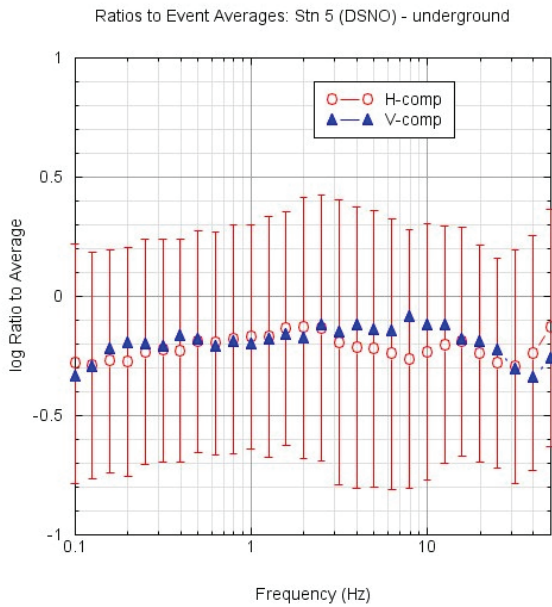


Figure 22: Log ratios for response spectra at surface Station 5 (DSNO) relative to event averages, for horizontal (H) and vertical (V) components.

Overall, the response spectra data indicate that amplitudes are somewhat lower at underground sites than those on the surface, especially on the horizontal component. But there is a very large variability, with interpretation further hampered by intermittent noise at all stations. The effect of the different cavity sizes at the different underground stations may also contribute to the variability. This means that to confidently establish the relative ratios between stations will require collection of a greater number of events. The number of events is important, as the standard error of the mean is the standard deviation of observations divided by the square-root of the number of observations, N . As N grows, the standard error of the mean will decrease, allowing us to more confidently establish the overall trends, even though variability will remain high. At present, the ratios are based on about a dozen regional events, so the standard errors of the mean are >0.1 log unit, which is of the same order as observed differences. By doubling the number of observations, we can reduce the standard error to values less than observed differences, and better establish these noted trends.

5. HIGH-FREQUENCY DECAY PARAMETER, KAPPA

In recorded ground motions on the surface, amplification of horizontal components through the near-surface velocity gradient is offset by decaying amplitudes at higher frequencies due to anelastic losses in the medium, probably from small-scale inhomogeneities. This high-frequency loss of energy is typically modeled by the parameter kappa (Anderson and Hough 1984). It is distinguished from broader transmission losses across large distances (which are inversely proportional to regional quality factor, Q) in that kappa (κ) corresponds to the high-frequency decay trend at near-source distances. It is sometimes referred to as κ_0 for this reason (to distinguish it from the apparent kappa at large distance, which is due to both κ_0 and Q effects). In this study, when we refer to kappa, it is the κ_0 parameter we are discussing. Kappa is an important ground-motion parameter in the development of ground-motion prediction equations, and in seismic hazard studies, because it acts to decrease high-frequency amplitudes and thus peak ground accelerations.

The form of the decay of spectral amplitudes at high frequencies is that Fourier amplitudes are proportional to the factor $\exp(-\pi f \kappa)$, where f is frequency. Without the effects of kappa, the Fourier displacement spectrum (FD) of earthquake signals should be flat (ie. constant with frequency) at near-source distances, for frequencies below the corner frequency of the earthquake, which is a function of earthquake size (Brune, 1970, Boore, 1983). (At near-source distances, Q effects are negligible.) For the small earthquakes ($M < 3$) that dominate this study, typical corner frequencies will be in the range from 10 to 20 Hz (Atkinson, 2004). Therefore, we can determine kappa by plotting $\log(\text{FD})$ versus frequency. The slope of this line will be $= \pi \kappa / 2.3$ (when plotting base10 logs), and thus kappa is just the slope divided by the factor 1.366.

A complication is that FD is contaminated by noise at low frequencies for small events. Noise plots (such as Figure 7) indicate typical noise levels for $\log \text{FD}$ of about -5 at 1 Hz, decreasing to -7 at 10 Hz. Thus when we examine plots of $\log \text{FD}$ versus frequency, as shown in Figure 23 for small local events recorded at 46SNO, the shape of the curve at frequencies below about 2 Hz is just dominated by noise. However, the linear trend between about 2 Hz and 10 Hz should be indicative of kappa, as these spectra are generally above the noise in this frequency range. For each small local earthquake (Table 1), we fit $\log \text{FD}$ versus frequency in the frequency range from 3 to 10 Hz to determine kappa at each station. Kappa values are similar for the

horizontal and vertical components. Their values for each station, when averaged over all events, are as follows:

Stn 1 (SSNO)	surface	$\kappa = 0.06$
Stn 2 (11SNO)	surface	$\kappa = 0.04$
Stn 3 (46SNO)	underground	$\kappa = 0.03$
Stn 4 (LSNO)	underground	$\kappa = 0.02$
Stn 5 (DSNO)	underground	$\kappa = 0.03$

The variability is high, so that these values are not well determined. They appear to indicate higher kappa on the surface, which is what we would expect from the idea that high-frequency attenuation is likely a site effect (Hanks, 1982). However, the values indicated for kappa are surprisingly large. Typical kappa values for ENA rock sites are about 0.002 or less (Atkinson, 1993; Atkinson and Boore, 2006). The observed values in the range of 0.02 to 0.06 are more typical of California soft-rock sites (Boore and Joyner, 1997). Further, at underground sites, near-zero kappa might have been expected, if it is truly a site effect. The observation of significant kappa at both surface and underground sites, based on study of the small local events, suggests it could be a source effect rather than a site effect. Kappa found here may differ from results of previous studies due to the small magnitude of the events studied, or other factors. In particular, most sources studied here are mining induced, and this may be significant. This requires further investigation, as it is an important factor that may limit high-frequency amplitudes.

Figure 24 further examines the high-frequency decay of spectra by plotting the average value of log FD, for several small local earthquakes, versus frequency. This plot appears to confirm that there is a significant decay slope, for both vertical and horizontal components; it appears to be slightly steeper for surface stations than those underground, confirming the results found above by averaging kappa at each station over all events.

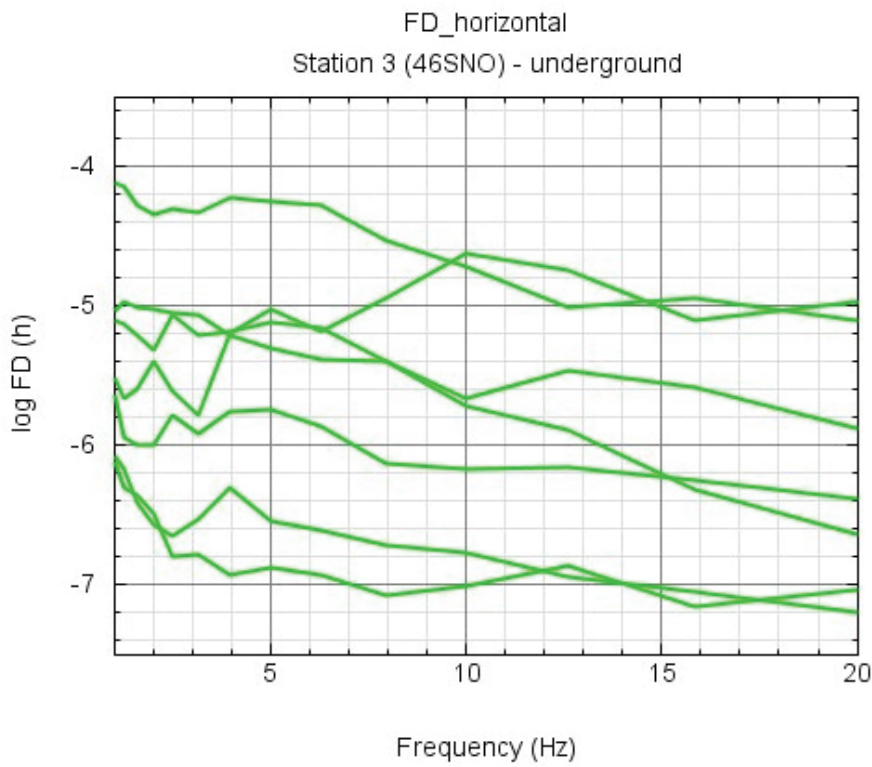
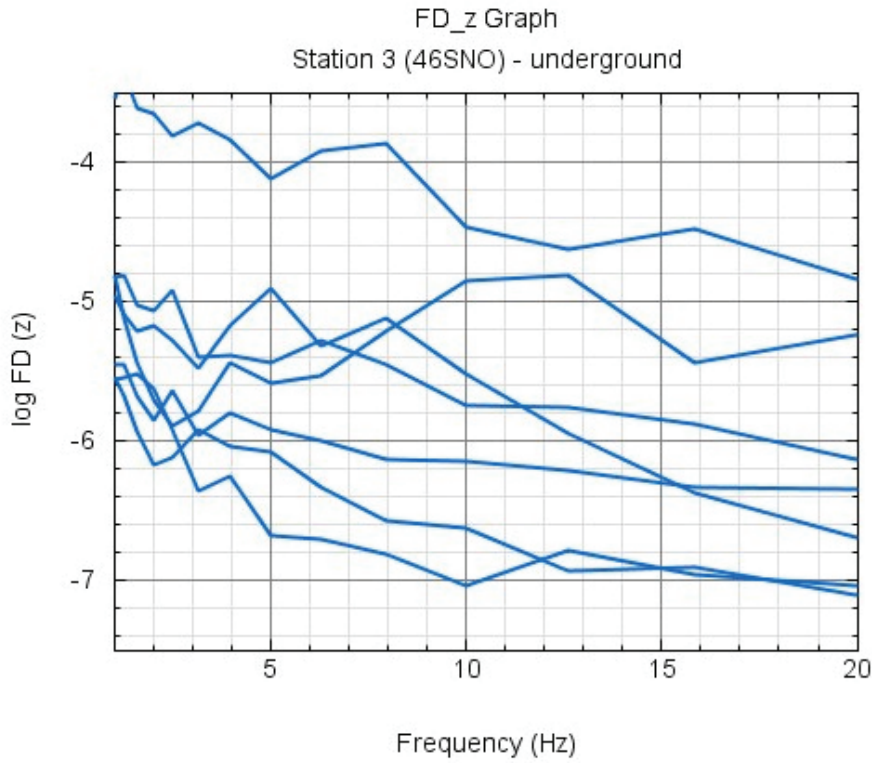


Figure 23: Typical behaviour of Fourier displacement spectra for small local earthquakes for vertical (top) and horizontal (bottom) components: Station 3 (46SNO)

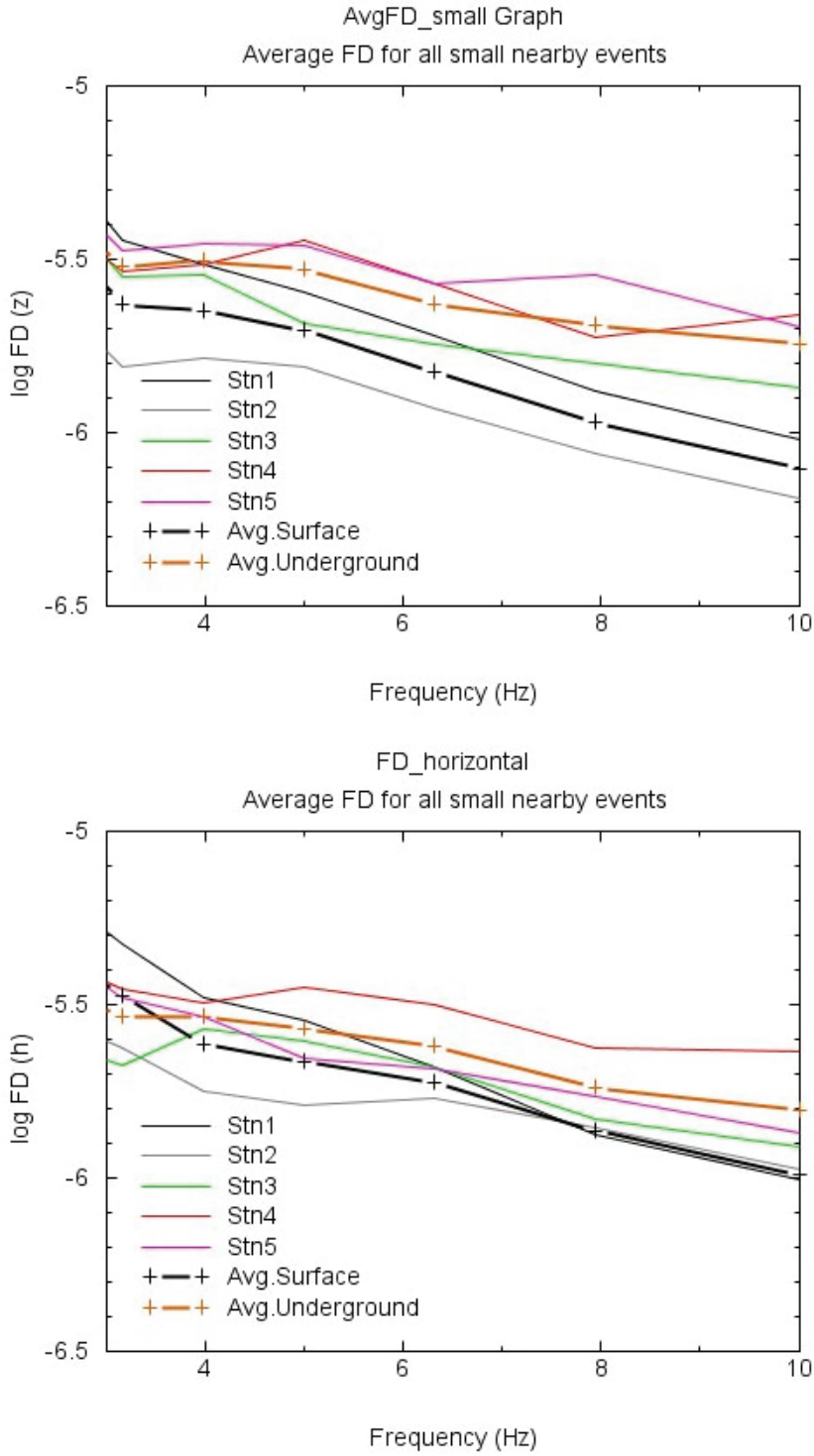


Figure 24: Average high-frequency decay (3-10) Hz for surface and underground stations, on vertical (top) and horizontal (bottom) components.

6. IMPLICATIONS OF GROUND MOTIONS FOR STRESS DROP PARAMETER

In this 1st year of study, there was time for only limited modeling of the source parameters of events, such as the seismic moment and stress drop. Initial estimates of moment magnitudes were made based on long-period spectral displacement levels, corrected to source using the attenuation model of Atkinson (2004), looking just at frequencies for which the displacement spectrum appears to be above the noise. These estimates were made using the same procedures as for the Lively earthquake sequence, as described in Appendix 1. The small local events, which had Nuttli magnitude (MN) in the range from 1.4 to 2.8, appear to have moment magnitudes (**M**) in the same range. However, there is significant scatter in the relationship between **M** and MN, as shown on Figure 25, with estimates being very different for a few events.

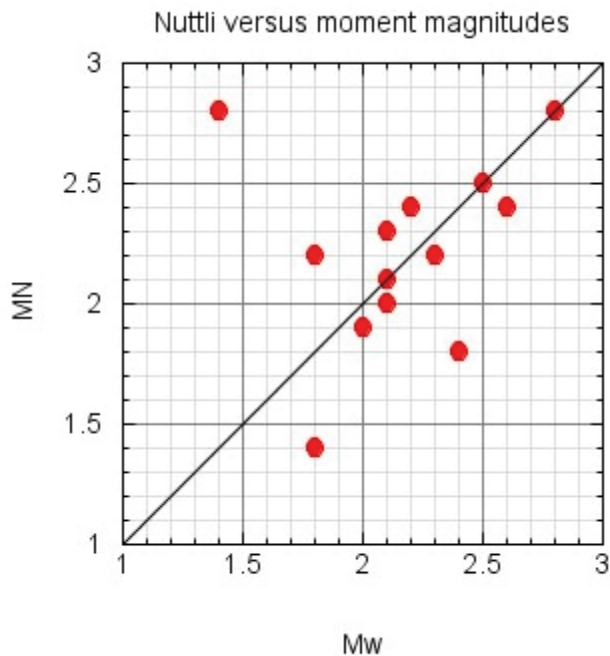


Figure 25: Correlation between MN (Nuttli magnitude) and preliminary estimates of M (moment magnitude).

With these estimate of moment, very preliminary stress drop estimates were made based on high-frequency spectral levels (with procedures as described in the Appendix 1). Stress drop estimates scatter widely, from <10 bars to about 200 bars, with most events having very low stress drops (<50 bars). However, if the kappa factor is significant, these stress drops may be underestimates, due to trade-offs between stress drop and kappa. Further modeling of the spectra to better determine source parameters, by using a simultaneous inversion for the moment, stress drop, and kappa are recommended for next year's studies. The preliminary findings suggest that stress drop parameters are generally low for small local events, and this will act in conjunction with kappa to limit high-frequency ground-motion amplitudes at underground sites.

7. CONCLUSIONS AND FUTURE WORK

7.1 CONCLUSIONS

The primary conclusions of the first year of the PUPS project are as follows:

1. Monitoring in the underground environment is challenging, and local noise from mining activities means that not all recorded signals are useable. Nevertheless, good signals are recorded at several stations for most significant local and regional events. The quietest and most reliable of the underground stations appears to be 46SNO (located in the satellite lab), while LSNO (located near a latrine along the drift between the clean lab and the elevator shaft) is the noisiest station. Response of the 2 surface stations differ significantly from each other, as does response of the underground stations. Further work is required to identify the quietest possible sites, and move stations if necessary to optimize their locations. This should be undertaken near the beginning of Year 2.
2. Ground motions appear to be lower at underground sites than on the surface, but this trend is subject to great variability, and is not as clearly indicated as might have been expected. Further monitoring is required to better establish the overall trends, by reducing the standard error of estimated differences through an increased number of observations.
3. There is a greater difference between the horizontal and vertical component amplitudes for surface sites than those underground, as would be expected based on the effect of the near-surface velocity gradient. Underground, horizontal and vertical component amplitudes are similar.
4. The inferred high-frequency decay parameter, kappa, as estimated from small local events, is larger than expected – about 0.05 for surface sites and 0.03 for underground sites. This suggests that kappa, at least for these small events, may be largely a source effect, because if it were a site effect we would expect to observe kappa values not significantly different from zero on the underground sites. This conclusion may be influenced by the fact that most recorded events are mining induced.
5. Stress drop estimates from the events are low (average <50 bars). Low source stress for shallow local events, in conjunction with a significant kappa, may act to limit high-frequency amplitudes experienced at underground sites from such events.

7.2 FUTURE WORK

The PUPS experiment at SNO is providing valuable new information on ground motions in underground environments. The recording environment is challenging as it is an operating mine and thus subject to frequent bursts of seismic noise, which can overwrite signals and complicate analysis. This means that not all potential events are usefully recorded on all stations. A longer monitoring period is required to compensate for this factor. Furthermore, there is great variability of results from one event to the next, and thus a significant number of events are required to establish average overall trends.

Some of the results of the analyses of the data collected in the 1st year are unexpected, and will require further data and analysis to fully interpret. It is recommended to continue monitoring for an additional 1 year period, along with further analysis. This will take advantage of the effort and investment that has already been expended in setting up the experiment and developing analysis procedures. All 5 instruments are in place and operating satisfactorily, despite the

operational noise constraints imposed by the mining environment, and data processing procedures are well established; thus continuation of the experiment is straightforward.

In the second year of the project, continued monitoring is expected to record another 10 to 20 local small-magnitude events ($M < 3$ at $R < 30$ km). Analysis of these signals will strengthen or refine our initial conclusions regarding the relative differences between surficial and underground signals. Using additional signals is important, as the 1st year of study revealed a high inter-event variability of results; given the large standard deviation, a large number of observations is required to establish the mean trends with confidence. The additional local events will also improve our estimates of kappa and source parameters of small events, for the same reasons. It is also possible that we will record a significant regional event, as was the case in the 1st year, providing further scope for the project. Finally, the 2nd year will allow time to develop additional analysis techniques to better handle some of the noise issues involved with the data. With the additional data, further modeling of the source spectra of small events should be performed, to simultaneously model moment, stress drop and kappa. This may provide further insights into the source spectra of recorded events.

A new line of study that is recommended, not part of the 1st year work, is to take advantage of the nearby regional POLARIS recordings at Sudbury (and also at more distant locations for the few largest events) to study ground-motion attenuation near the earthquake source (distances < 50 km). This is a very important topic for seismic hazard analysis. Recent studies by Atkinson and Boore (2006) predict a much more rapid decay of ground motions in the first 50 km from the source than had been assumed previously. Their new ground-motion relations lead to much lower seismic hazard estimates at high frequencies than previous relations, for this reason. CNSN signals at Sudbury (SUNO station) for all of the micro-events analyzed in both Year 1 and 2 will be processed, and an empirical study of near-source attenuation made. These results can be used to test or validate the Atkinson and Boore (2006) ground-motion attenuation model, and improve confidence in its use for seismic hazard estimates.

Analyses of teleseismic signals will be carried out in Year 2 to better establish low-frequency trends. Very preliminary analyses of these signals were conducted in the first year, but there was not adequate time to fully investigate these results. It should be possible to use the teleseismic signals, in concert with the local results, to establish a frequency below which the underground and surface signals are the same. At higher frequencies, the waves should “see” the cavity and its size. If these trends can be identified more clearly, then it would enable more detailed modeling by NWMO engineers of the effect of cavity size on ground motions, including validation studies of numerical models.

It would also be useful to perform additional modeling of the near-source signals recorded during the Lively earthquake and its aftershocks, to try to better understand the enigmatically low motions recorded closest to the event (at DSNO). This would require further analysis work, and examination of additional aftershock signals that were recorded but not analyzed in detail in the 1st year.

In summary, the work tasks proposed for Year 2 of the PUPS project are as follows:

1. Process data from all new local and regional events.
2. Refine analysis of the ratios between spectra (Fourier and response spectra) for underground and surficial sites. Use the additional signals to better define the mean trends. Perform additional research to interpret the results.

3. Refine the analysis of the high-frequency decay parameter, kappa, at underground and surficial sites. First year results suggest, unexpectedly, that kappa is fairly similar, and significant, for both underground and surficial sites. Thus it may be a property of the earthquake source, rather than simply a site parameter, as previously believed. Further verification and interpretation of this finding is important, as it implies that high-frequency motions underground may be limited by the kappa effect.
4. Determine source parameters (moment and stress drop) for all new recorded local events. Refine the analysis of source parameters to simultaneously model moment, stress drop and kappa.
5. Perform a study of attenuation near the earthquake source, using a combination of signals recorded at SNO and on nearby CNSN stations, in particular SUNO.
6. Analyze teleseismic signals to determine the low-frequency behaviour of the ratio of underground to surficial spectra. This was only just begun in Year 1 and much more analysis and interpretation is needed.
7. Perform additional modeling of the near-source signals recorded during the Lively earthquake sequence to better understand near-source ground motions. This is an important topic for underground storage facilities. There has not yet been time to fully explore these motions, as the recording of near-source motions was an unexpected bonus, and thus no near-source analyses had been planned for Year 1. These analyses should be undertaken in more detail in Year 2.

ACKNOWLEDGEMENTS

We wish to thank the Sudbury Neutrino Observatory (SNO) and INCO for providing various supports throughout the course of the project. The analysis of the Lively earthquake involved collaborative work with scientists from the Geological Survey of Canada; in particular the results reported in Chapter 3 are taken from a paper by Atkinson, Kaka, Eaton, Bent, Peci and Halchuk which will be published shortly in *Seismological Research Letters*. We are grateful for their collaboration.

REFERENCES

- Anderson, J. and S. Hough (1984). A model for the shape of the Fourier amplitude spectrum of acceleration at high frequencies. *Bull. Seism. Soc. Am.*, **74**, 1969-1993.
- Atkinson, G. (1993). Notes on ground motion parameters for eastern North America: Duration and H/V ratio. *Bull. Seism. Soc. Am.*, **83**, 587-596.
- Atkinson, G. (2004). Empirical attenuation of ground motion spectral amplitudes in southeastern Canada and the northeastern United States. *Bull. Seism. Soc. Am.*, **94**, 1079-1095.
- Atkinson, G., and D. Boore (1995). New ground motion relations for eastern North America. *Bull. Seism. Soc. Am.*, **85**, 17-30.
- Atkinson, G. and D. Boore (2006). Ground motion prediction equations for earthquakes in eastern North America. *Bull. Seism. Soc. Am.*, **96**, 2181-2205.

- Beresnev, I. and G. Atkinson (1997). Shear wave velocity survey of seismographic sites in eastern Canada: Calibration of empirical regression method of estimating site response. *Seism. Res. L.*, **68**, 981-987.
- Boore, D. (1983). Stochastic simulation of high-frequency ground motions based on seismological models of the radiated spectra. *Bull. Seism. Soc. Am.*, **73**, 1865-1894.
- Boore, D. and W. Joyner (1997). Site amplifications for generic rock sites. *Bull. Seism. Soc. Am.*, **87**, 327-341.
- Brune, J. (1970). Tectonic stress and the spectra of seismic shear waves from earthquakes. *J. Geophys. Res.*, **75**, 4997-5009.
- Hanks, T. (1982). f_{max} . *Bull. Seism. Soc. Am.*, **72**, 1867-1879.
- Siddiqi, J. and G. Atkinson (2002). Ground motion amplification at rock sites across Canada, as determined from the horizontal-to-vertical component ratio. *Bull. Seism. Soc. Am.*, **92**, 877-884.

Appendix 1 – THE LIVELY EARTHQUAKE SEQUENCE

(preprinted from Atkinson et al. *Seism. Res. L.*, 2007)

A very close look at a moderate earthquake near Sudbury, Ontario

for SRL Eastern Section pages: Gail M. Atkinson, SanLinn I. Kaka, David Eaton, Allison Bent, Veronika Peci, and Stephen Halchuk

Sept. 28, 2007

Abstract

A mining-induced earthquake of MN4.1 at a depth of 2.35 km, at Lively, Ontario, near Sudbury, offers a rare close-up view of a moderate event in an intraplate setting. It was recorded by 5 three-component broadband seismographic stations at hypocentral distances from 0.4 to 3 km, as well as by regional seismographs at distances from 22 to hundreds of km. The closest station to the event is within the Sudbury Neutrino Observatory (SNO) lab, which is 2 km beneath the surface, and about 300 m above the event. Physical inspection of the hypocentral area was possible due to its location in the Creighton mine. The close proximity of this station to the event enabled detection of abundant small aftershocks (70 during the first 12 hours) and recording of rarely-seen near-field components of the seismic wavefield.

We analyze local and regional recordings of the Lively event. An interesting finding is that when regional waveforms are used in a moment tensor inversion, the resulting best-fit depth (7 km) exceeds the known depth (2.35 km) of the event. However, a careful examination suggests that the degree of fit to the observed waveforms is not degraded significantly if the moment tensor solution is forced to a shallower depth. Regional waveform modeling is an alternative method for obtaining focal depths for moderate events. Regional waveform modeling provides a well-constrained estimate of focal depth for the Lively event, in the range of 2.5 to 3 km, in good agreement with its known depth.

The mainshock had a moment magnitude of 3.7 to 3.8 and a Brune stress drop near 20 bars. Recorded ground motions agree with the values predicted by regional ground-motion equations for an event of this magnitude and stress drop, over epicentral distances ranging from 0 to hundreds of km. Subsurface ground-motions, recorded at distances from 0.4 to 1 km above the hypocenter, were a factor of 3 to 10 lower than the apparent source spectra (defined at a reference distance of 1 km) as obtained from hard-rock recordings made on the surface.

Introduction

A shallow moderate earthquake of MN4.1 occurred near Sudbury, Ontario, at 07:22:55 UTC (02:22:55 local time) on Nov. 29, 2006. The event was located 6 km from Lively, Ontario, and was induced by mining activity at INCO's Creighton mine. INCO's in-mine monitoring system, and their subsequent visual inspection, places the event at 46.47 N 81.20 W, at a depth of 2.35 km. This event offers us a rare close-up view of a moderate earthquake, because it was recorded at close distances by five 3-component broadband POLARIS (Portable Observatories for Lithospheric Analysis and Research Investigating Seismicity; www.polarisnet.ca) seismographic stations that are installed above and within the Creighton mine. Two stations are located on the surface, near the epicenter, while there are three subsurface stations at depths of 1 to 2 km. The closest station to the event is within the Sudbury Neutrino Observatory (SNO) lab, which is 2 km beneath the surface, and about 300 m

above the event. The event caused no damage to the SNO lab, and only minor damage to the mine workings; there were no injuries. The event was widely felt in the Sudbury, Ontario region, as expected based on instrumental ShakeMaps (www.shakemap.carleton.ca) and confirmed by internet intensity reports (www.earthquakescanada.ca). The mainshock was followed by two significant aftershocks at 2:36 (MN 2.0) and 2:38 (MN 3.1) local time, and by many smaller aftershocks. In addition to the near-source records, this event was well-recorded regionally at distances from 20 km to hundreds of km, by the seismographic stations of the Canadian National Seismographic Network (CNSN) and (POLARIS). Figure 1 shows the location of the Lively event in relation to regional seismographic stations; the nearest regional station is CNSN station SUNO, 22 km away. In this note, we provide a preliminary examination of the recorded ground motions from this event, and discuss their implications for our understanding of source and attenuation properties in eastern North America (ENA).

Tectonic Setting and Earthquake Sequence

Tectonic Setting

One of the world's deepest underground mines (> 2 km), the Creighton Mine has produced more than 160 Mt of Ni-Cu ore since opening in 1901. The mine is located along the southern periphery of the Sudbury Structure, interpreted by most researchers as a relict giant impact (e.g., Riller, 2005; Grieve and Therriault, 2000). The structure consists of a differentiated melt sheet (Sudbury Igneous Complex) overlain by impact breccias and post-impact sedimentary rocks (Pye et al., 1984). The structure, together with older Precambrian rocks of the Canadian Shield, were deformed by post-impact orogenic processes to produce a large-scale asymmetric synform (Milkereit et al., 1992). Like most other ore deposits in the Sudbury region, the Creighton Mine is situated near the base of the impact melt sheet, near its contact with the footwall. The SNO laboratory, where the closest seismic instruments are located, is situated within a massive igneous unit (Norite) within the Sudbury Igneous Complex.

The Lively Sequence

The Lively earthquake sequence was comprised of the MN (Nuttli magnitude) 3.8 mainshock and a sequence of aftershocks. Accurate characterization of aftershock statistics is important for hazard calculations, particularly in a mining environment where they may determine protocols for re-entry into a mine following a significant mining-related earthquake. In this case, two moderate aftershocks occurred 13 and 15 minutes after the mainshock, respectively. Although these larger aftershocks were observed at regional distances, most other aftershocks were too small to be observed at regional distances and were recorded only by local instruments. The close proximity of the deep underground seismometer at SNO enabled the measurement of a rich record of aftershock activity at the MN > 0 level that would otherwise be largely undetected. By examining the raw seismic data from the deep SNO site, we measured the arrival time and amplitude of 70 aftershocks that occurred within a 12-hour period after the mainshock.

Figure 2 shows the rate of observed aftershocks during the initial 12-hour period following the mainshock, measured using a moving 1-hour time window. We fit the observed trend using a modified form of Omori's Law (Shcherbakov et al., 2004):

$$N(t, M) = \frac{1}{\tau \left(1 + \frac{t}{c}\right)^p} \quad (1)$$

where t is time since the mainshock, M is magnitude threshold (here estimated to be $M_N \sim 0$), $\tau(M)$ is the reciprocal of the initial rate of aftershocks, $c(M)$ is the characteristic decay time and $p(M)$ is a parameter that controls the rate of decay of aftershocks. We used a grid search method to find the values of τ , c and p that minimize the least-squares misfit with respect to the observed aftershock rate. The resulting curve (Figure 2) fits the overall aftershock trend reasonably well, but fails to reproduce several conspicuous peaks in aftershock activity that occurred 2-8 hours after the mainshock. In order to fit this aftershock decay pattern, a more complex model is required, such as the epidemic-type aftershock sequences model (ETAS) which includes triggering events within a cascading sequence (Ogata, 1988; 1999). We remark that, of the three parameters needed for the generalized Omori representation of aftershock rate, only τ is well constrained by the data considered here. Large tradeoffs between c and p mean that other combinations of these parameters provide nearly equivalent fits to the data. Thus, although more work is needed to characterize the aftershock model more accurately, these preliminary results illustrate the potential insights into aftershock processes that may be afforded by the near-field aftershock recordings obtained here.

Ground-motion Data from the Lively Earthquake

Instrumental Data

Figure 1 shows the locations of regional stations in relation to the Lively earthquake. Regional stations typically sample at 40 to 100 Hz. The 5 SNO stations are located beneath the symbol marking the event location; the sample rate for these local stations is 200 samples/sec. The 2 local stations on the surface (SSNO and 11SNO) are sited on hard rock, while the 3 subsurface stations (DSNO, LSNO and 46SNO) are within underground openings, all in hard rock, that are >4 m in diameter (both directions) and approximately 3 m in height. Table 1 shows the distances from the MN4.1 event to SUNO and the five SNO stations. Figure 3 plots example seismograms. Note that the very short duration of the records at SNO (about 1 sec) limits the analysis of the local seismograms to frequencies greater than ~ 2 Hz. Furthermore, the absolute timing of the underground stations is not accurate, due to the lack of availability of a GPS time signal underground.

Regional and local data were processed using procedures described by Atkinson (2004). Briefly, the window of strongest shaking (shear window, including direct, reflected and refracted phases) was selected for each record, and a 5% taper was applied at each end of the window. The Fourier spectrum of acceleration was determined, correcting for instrument response. (Fourier displacement spectra were also calculated.) The spectra were smoothed and tabulated in increments of 0.1 log frequency units, for log frequencies of 0 to 1 (eg. 1 to 10 Hz). Instrument-corrected acceleration time series were used to compute response spectral amplitudes (5% damped pseudo-acceleration, PSA). In computing the instrument-corrected time series, the records were baseline corrected, and Butterworth filtered (4th order). Filter frequencies for the regional records are 0.1 Hz to 50 Hz, while the local records were filtered from 2 Hz to 90 Hz, due to their higher sampling rate, and short duration.

Felt Intensity Data

The Lively event was widely felt in the Sudbury region, with the maximum reported individual estimate of modified Mercalli intensity (MMI) being VI (6). 124 observations were reported to the Geological Survey of Canada's community internet intensity program

(www.earthquakescanada.ca), which is a minor modification of the U.S. Geological Survey's "Did You Feel It?" program (modifications allow users to report location by postal code rather than zip code, for example). Figure 4 shows the intensity observations. These were binned by distance to establish stable mean trends, as discussed by Atkinson and Wald (2007); the mean binned intensities near the source are approximately IV (4). The mean binned intensities were used to infer MMI-based estimates of PGA and PGV, by inverting the following equations of Atkinson and Kaka (2007) to solve for PGA and PGV:

$$\text{MMI} = 2.65 + 1.39 (\log \text{PGA}) \quad (\text{MMI} < 5) \quad (2a)$$

$$\text{MMI} = 4.37 + 1.32 (\log \text{PGV}) \quad (\text{MMI} < 5) \quad (2b)$$

Source and Attenuation Processes

Analysis of Fourier Spectra

The processed spectral data are used to evaluate the overall source and attenuation processes for the Lively event. We can correct the Fourier acceleration spectral amplitudes at each station back to the reference distance of 1 km, using the trilinear spectral ENA attenuation model of Atkinson (2004). This provides an apparent source spectrum from each station, given by:

$$\log A_{src}(f) = A_{obs}(f) + 1.3 \log R + c_4(f) r \quad \text{for } r \leq 70 \text{ km} \quad (3a)$$

$$\log A_{src}(f) = A_{obs}(f) + c_4(f) r + 1.3 \log (70) - 0.2 \log(r/70) \quad \text{for } 70 < r \leq 140 \text{ km} \quad (3b)$$

$$\log A_{src}(f) = A_{obs}(f) + c_4(f) r + 1.3 \log (70) - 0.2 \log (140/70) + 0.5 \log (r/140) \quad \text{for } r > 140 \text{ km} \quad (3c)$$

where r is hypocentral distance, $A_{obs}(f)$ is the observed acceleration spectrum at the station, and $c_4(f)$ is the coefficient of anelastic attenuation from Atkinson (2004). (Note: The anelastic attenuation coefficient c_4 is of positive sign in this formulation, increasing from 0 at $f = 0.2$ Hz to 0.00271 at 20 Hz. The geometric spreading coefficient is 1.3 in the first 70 km.) The values of $\log A_{src}(f)$ are averaged over all stations to obtain the mean apparent source spectrum and its standard deviation. Only stations sited on hard rock, on the surface, were used to obtain the apparent source spectrum; the subsurface recordings will be compared to this spectrum later.

Figure 5 shows the apparent source spectrum of acceleration ($r = 1$ km) for the event, for both the horizontal and vertical components. The displacement spectrum (obtained by dividing the acceleration spectrum by $(2\pi f)^2$) is also shown, for the vertical component. The vertical component is interpreted to be representative of the unamplified horizontal component (Atkinson, 2004; Beresnev and Atkinson, 1997; Siddiqi and Atkinson, 1999), as the amplification on the vertical component is considered negligible for hard rock sites. The horizontal component shows minor amplification relative to the vertical, due to the impedance effects of the crustal shear wave velocity profile; velocities at depth (3 km) are likely about 3.5 km/s, while those near the surface are typically 2 to 3 km/s (Beresnev and Atkinson, 1997); this would produce an amplification of about a factor of 1.3, according to the quarter-wavelength approximation (Boore and Joyner, 1997). The observed spectrum follows the simple omega-squared model (Brune, 1970) well. From the vertical-component Fourier displacement (FD), we infer a long-period spectral level of 0.02 cm-s ($\log \text{FD} = -1.7$). The seismic moment (M_0) can be estimated from (Boore, 2003):

$$FD = C M_0 \quad (4)$$

where $C = (0.55) (0.71) (2.) / (4 \pi \rho \beta^3)$. (Note: the constants in the numerator represent radiation pattern, partition onto two horizontal components and free surface amplification, respectively.) We assume $\rho=2.8 \text{ g/cm}^3$ and $\beta = 3.5 \text{ km/s}$. The moment magnitude ($M = 2/3 \log M_0 - 10.7$; Hanks and Kanamori, 1979) obtained from the displacement spectrum is then $M = 3.8$ ($M_0 = 4.76E21 \text{ dyne-cm}$). This is in good agreement with the moment tensor solution for this event, presented in the next section. Under the Brune (1970) model, the acceleration spectra can be written (Boore, 2003):

$$A_{src}(f) = C M_0 (2 \pi f)^2 / (1 + (f/f_0)^2) \quad (5)$$

where f_0 is the corner frequency, which is related to the stress drop by (Boore, 2003):

$$f_0 = 4.9E6 \beta (\Delta\sigma/M_0)^{1/3} \quad (6)$$

for $\Delta\sigma$ in bars, M_0 in dyne-cm and β in km/s. Thus we can use the high-frequency level of the acceleration spectrum, along with the inferred moment, to estimate stress drop. Based on the vertical component, we would estimate a high-frequency level of approximately 0.8 log units. The horizontal component high-frequency level is about 1.1 log units, but has likely been amplified by about a factor of 1.3 (0.1 log units) by the impedance gradient. Overall then, our best estimate for the high-frequency level is 0.9 log units, resulting in an estimated corner frequency of 2.86 Hz, and a stress drop of 22 bars using Equations 3 and 4. In comparison, studies of regional ENA earthquakes of small-to-moderate magnitude, in which the stress drop is calculated using the same procedure as that described above, typically suggest stress drops of 100 to 200 bars for events of $M>4$ (Atkinson, 2004). However, these same studies also reveal a decreasing trend in stress drop value with decreasing magnitude, with typical values for an event of $M3.8$ being in the range of 30 to 80 bars. Thus the value of 22 bars obtained for the Lively event is a relatively low stress drop, but not anomalous for an event of this magnitude.

An important issue in evaluating the robustness of the apparent source spectra is the goodness-of-fit of the assumed attenuation model to the trends actually shown by the data. Figure 6 plots the inferred source levels (by Equation 1) for each station as a function of distance, for two selected frequencies. There are no trends of the inferred source levels with distance, which corroborates the assumed attenuation model. In particular, the source levels inferred from the closest stations are not significantly different than those inferred from stations hundreds of km away.

Moment Tensor Analysis

A moment magnitude of 3.8 is inferred for this event based on the long-period level of the apparent source spectra at local to regional distances. A more robust measure of the seismic moment can be obtained from a moment tensor inversion. Figure 7 shows the moment tensor inversion, based on modeling of the waveforms at 5 stations. A standard eastern Canada velocity model (Brune and Dorman, 1963, with crust thickened to 40 km) was used at all stations. At each station, a frequency range was selected for the modeling; the signal to noise ratio was checked, and the inversion code used only those frequencies that have a signal/noise ratio >2 . Each component was assigned a weight in the inversion based on its judged quality. For example VLDQ is weighted 1, 1, 0 which means that the vertical and radial are given full weight and the tangential is not used; the tangential component was discounted because it looks noisy, although the actual fit to this component is similar to that achieved for the other components. In displaying the results, the misfit is calculated even for the components that weren't used in the inversion, which tends to make the misfit appear large. If the misfit is

recalculated using only the components that were used in the inversion, it is reduced from 0.69 to 0.36, which is considered a reasonably-good fit. The moment magnitude of 3.7 derived from the moment tensor inversion is in good agreement with the estimate of 3.8 obtained from the regional seismographic data.

On the focal mechanism plot of Figure 7, the dashed lines are for the best fit double couple and the shading is for the complete moment tensor solution. The CLVD (compensated linear vector dipole) component, which gives an indication of the non-double couple component of the source, is a bit high. The high CLVD could be an indication that there was a non double couple component to the rupture, possibly related to the mining environment. However, caution should be taken not to over-interpret it. The CLVD could also result from noise in the data, not unrealistic given that we are modeling long periods for a relatively small earthquake. The best depth from the moment tensor inversion is about 7 km, according to the misfit plot as a function of depth on Figure 7 (including all components). However, the depth is not well constrained. Moment tensor inversions are often not good at resolving very shallow depths because of the longer periods modeled (Ekström and Dziewonski, 1985). In this case, the depth of the event is known from the mine monitoring and inspection. The depth can be more accurately estimated from seismic records based on the focal depth modeling method discussed in the next section. Note that if the depth is forced to be shallower in the moment tensor inversion, the best fit occurs for a 3 km depth and the calculated thrust component will be higher (Figure 7 inset). The non-double couple component also increases to 49%, which would normally be an indication of a poorer fit but for reasons previously discussed should be interpreted with caution in this case. Comparing the misfit on a station by station basis, by forcing the solution to a shallower depth there is no change (no change being defined as less than 0.01 difference in either direction) for OTT, KAPO and BUKO, a slight improvement (0.03) for 3 km at SADO and a stronger preference (0.21) for 7 km at VLDQ. A comparison of individual component misfits reveals a similar distribution, with no change for VLDQ-R, OTT- all components, SADO-Z, KAPO-R and BUKO-R. A 3 km depth improves the fit at SADO-R and T, BUKO-Z and KAPO-T with a mean improvement of 0.09. The 3 km depth deteriorates the fit at VLDQ-Z and T, BUKO-T and KAPO-Z with a mean difference of 0.22. In summary, it appears that while the 7 km depth does provide a better overall fit to the long-period waveforms, the well-constrained shallower depth determined from the local data does not lead to a significantly worse fit. We also note that the thrust mechanism obtained using the shallower depth is more similar to the focal mechanisms of other earthquakes in western Quebec and eastern Ontario than is the predominantly strike-slip mechanism obtained with the depth of 7 km.

Focal Depth Analysis from Regional Waveforms

The depth of the Lively event is well constrained at 2.35 km by very local seismic records in the mine, and has been confirmed by inspection of the focal area by INCO. It is nevertheless of interest to see how well the depth can be inferred from regional seismographic information, as this bears on the reliability of methods of estimating depth for the more usual case where we have few or no near-source records. A particularly promising method of estimating focal depths in regions of sparse instrumental coverage is the regional depth phase modeling approach described by Ma and Atkinson (2006). This method is based on modeling the regional depth phases sPg, sPmP and sPn, with their reference phases Pg, PmP and Pn, respectively. These phases are often clearly visible on regional seismograms. The method is based on the calculation of synthetics using the reflectivity method (Randall, 1994) with a default focal mechanism and a default crustal model (eg. Mereu *et al.*, 1986). By comparing the synthetics with the observations for selected station distances over a reasonable range of focal depths, the depth that provides the best agreement (in relative arrival times) between the synthetics and observations can be identified. For this event, depth information comes from the sPg phase.

Vertical displacement waveforms recorded at distances from 162 to 296 km that show this phase clearly were selected. Synthetic waveforms were simulated in a suitable range of depths, in order to choose the depth at which the synthetic best matches the selected waveform. Four seismic stations, EEO, BUKO, SADO, CRLO, have been used to calculate the focal depth. The best fit for the synthetic with the observed data is at a depth range of 2.5 -3.0 km, just slightly larger than the known depth of 2.35 km. Figure 8 illustrates the fit for one of the stations (EEO). A well-developed Rg phase on many stations (including EEO) also supports the shallow depth.

Effects of near-field source terms

In an elastic medium, the n th component of ground velocity due to a point-dislocation source may be written as:

$$v_n(t) = \frac{a_{pq}}{4\pi\rho r^4} \int_{r/\alpha}^{r/\beta} \tau M_{pq} \dot{s}(t-\tau) d\tau + \frac{b_{pq}}{4\pi\rho\alpha^2 r^2} M_{pq} \dot{s}\left(t - \frac{r}{\alpha}\right) + \frac{c_{pq}}{4\pi\rho\beta^2 r^2} M_{pq} \dot{s}\left(t - \frac{r}{\beta}\right) + \frac{d_{pq}}{4\pi\rho\alpha^3 r} M_{pq} \ddot{s}\left(t - \frac{r}{\alpha}\right) + \frac{e_{pq}}{4\pi\rho\beta^3 r} M_{pq} \ddot{s}\left(t - \frac{r}{\beta}\right), \quad (7)$$

where r is distance, α , β and ρ are the P - and S -wave velocity and density of the medium, M_{pq} is the moment tensor, $s(t)$ is the source time function and a_{pq} , b_{pq} , c_{pq} , d_{pq} and e_{pq} are geometrical terms (see Aki and Richards, 1980, p. 79 for details). The first three terms in this expression represent near-field terms that decay as $1/r^4$ and $1/r^2$ respectively. These contribute significantly to the total ground motion only within a few wavelengths of the source and are generally neglected in the creation of synthetic seismograms. The last two terms decay as $1/r$ and represent far-field terms that are normally considered for modeling ground motion.

In the case of near-field records of the Lively earthquake, ground-motion observations are available at a fraction of the P - and S -wavelengths. For the dominant frequency produced by this earthquake (~ 1.25 Hz) at the closest stations (DSNO), near-field terms are similar in amplitude to the far-field terms. Figure 9(a) shows the unfiltered vertical-component recording of ground velocity at the DSNO station caused by the mainshock, after removal of the mean and normalization by its maximum value. To approximate the long-wavelength part of the source time function (Fig. 9b), we used:

$$\dot{s}(t) = \frac{1 - \cos(2\pi t/T)}{2}$$

with a period $T = 0.8$ s. Based on the moment tensor obtained from regional waveform modeling, we computed the near-field ground velocity without (Fig. 9c) and with (Fig. 9d) inclusion of the near-field terms. Since the seismograph is close to the focal depth, even the vertical record is dominated by shear-wave signals. The far-field shear-wave produces a waveform with the shape of the time derivative of the source time function given above. This waveform does not provide a satisfactory fit to the observed ground motion. However, interference between this and the near-field terms results in initial negative motion followed by longer duration positive signal (Fig. 9d), consistent with the observed data (Fig. 9a).

This example illustrates the significance of near-field terms in the ground-motion record at stations very close to the earthquake source. More detailed studies using inversion techniques may permit us to constrain the source time function more precisely.

Response Spectral Amplitudes

The response spectral amplitudes, showing how a single-degree-of-freedom oscillator would respond to the ground shaking, are plotted as a function of distance on Figure 10. The horizontal component of pseudo-acceleration (PSA) for 5% damping is shown, in comparison to various prediction equations that are used in seismic hazard and ShakeMap applications. Estimated PGA and PGV based on binned MMI observations (using the equations of Atkinson and Kaka, 2007, to convert MMI to PGA and PGV) are also plotted, and agree well with actual instrumental data.

The response spectral amplitudes are overpredicted by the Atkinson and Boore (2006) ground-motion relations for hard rock in ENA. This is not surprising, as the event had a stress drop of only 22 bars, while the Atkinson and Boore (AB06) relations are based on a median stress drop of 140 bars. The AB06 relations contain an adjustment factor that can be used to convert the equations to equivalent values for other stress drops. The predictions for 20 bars are shown on Figure 10, and agree quite well with the observations. The AB06 relations are based on an empirically-calibrated theoretical model of ground motions, and are mainly applicable to larger earthquakes ($M > 4$). By contrast, Kaka and Atkinson (2005) developed an entirely empirical ground-motion prediction equation, for use in Ontario ShakeMap applications, that is applicable to small-to-moderate events ($M < 5$). The Kaka and Atkinson (2005) relation is also shown on Figure 10. It matches the observational data from the Lively earthquake well. Thus the ground-motion amplitudes that were experienced in this event are consistent with our expectations for an event of this size, at distances from near-source to hundreds of km.

Subsurface Observations

A unique aspect of this dataset is the availability of observations from below the surface, within very hard rock, only a few hundred meters from the hypocenter. Figure 11 compares horizontal-component observations on the surface to those at depth, while Figure 12 provides the same plot for the vertical components. Note that the acceleration spectra are nearly constant with frequency over the range available (3 – 40 Hz), as the corner frequency of the event is about 2.8 Hz (Equation 6). In these plots, the surface observations (from SSNO and SNO11, which are very near the epicenter, and from SUNO, 22 km away) are corrected to a hypocentral distance of 1 km, using Equation (1). The average source spectrum at 1 km from all stations is also shown. The subsurface observations are at hypocentral distances of 0.4 to 1.3 km. They are *not* corrected to a distance of 1 km. The reason is that we are uncertain as to the appropriate distance correction in this case. The geometric spreading factor of 1.3 found by Atkinson (2004) applies to observations on the surface, from hypocentral distances of about 10 km and greater. It results from the travel of the waves through the crustal velocity structure. At close distances, below the surface, it would be reasonable to suppose that the theoretical geometric spreading factor of 1.0 for body waves might apply – although for the closest stations the near-field terms of Equation (7) may also need to be considered. However, it can be observed from Figures 11 and 12 that the closest underground station, DSNO (0.4 km), has lower amplitudes than the other underground stations, LSNO and 46SNO, both of which are at distances close to 1 km from the hypocenter. Thus any distance correction to normalize the records to a reference distance of 1 km would make little change to LSNO or 46SNO, while reducing the amplitude at DSNO.

Overall, from the comparison of surface and subsurface records, we can conclude that (i) the distance-corrected surface records are in agreement with our expectations based on the apparent source spectrum obtained from distant stations; and (ii) the subsurface records, which are at a distance close to the reference distance of 1 km for the surface records, have

amplitudes that are lower than those at the surface, by a factor in the range from 3 to 10. This may have important implications for ground motions experienced in underground waste repositories, and may also explain the lack of significant damage to the Creighton mine workings.

Conclusions

The mining-induced event near Lively, Ontario had a moment magnitude of 3.7 to 3.8 and a stress drop near 20 bars. The close proximity of deep underground sensors enabled recordings of numerous aftershocks and rarely-seen near-field components of the seismic wavefield. Overall, ground motions were as expected, according to the predictions equations of Kaka and Atkinson (2005) and Atkinson and Boore (2006) for an event of this magnitude and stress drop, at epicentral distances ranging from 0 to hundreds of km. Subsurface ground-motions, recorded at distances from 0.4 to 1 km above the hypocenter, were a factor of 3 to 10 lower than the apparent source spectra (defined at a reference distance of 1 km) as obtained from hard-rock recordings made on the surface.

Acknowledgements

The cooperation and invaluable assistance to our monitoring efforts given to us by the Sudbury Neutrino Observatory and INCO are gratefully acknowledged. We thank Eliza Richardson for her constructive review comments. Financial support for this study was provided by the Natural Sciences and Engineering Research Council of Canada, and by Ontario Power Generation/Nuclear Waste Management Organization.

References

- Aki, K. and P. Richards (1980). Quantitative Seismology: Theory and Methods. W.H. Freeman and Company, San Francisco.
- Atkinson, G. (2004). Empirical Attenuation of Ground Motion Spectral Amplitudes in Southeastern Canada and the Northeastern United States, *Bull. Seism. Soc. Am.*, **94**, 1079-1095.
- Atkinson, G. and D. Boore (2006). Ground motion prediction equations for earthquakes in eastern North America. *Bull. Seism. Soc. Am.*, **96**, 2181-2205.
- Atkinson, G. and S. Kaka (2007). Relationships between felt intensity and instrumental ground motions for earthquakes in the central United States and California. *Bull. Seism. Soc. Am.*, **97**, 497-510.
- Atkinson, G. and D. Wald (2007). Modified Mercalli Intensity: A surprisingly good measure of ground motion. *Seism. Res. L.*, in press.
- Beresnev, I. and G. Atkinson (1997). Shear wave velocity survey of seismographic sites in eastern Canada: Calibration of empirical regression method of estimating site response. *Seism. Res. L.*, **68**, 981-987.
- Boore, D. (2003). Prediction of ground motion using the stochastic method. *Pure and Applied Geophysics*, **160**, 635-676.
- Boore, D. and W. Joyner (1997). Site amplifications for generic rock sites. *Bull. Seism. Soc. Am.*, **87**, 327-341.
- Brune, J. (1970). Tectonic stress and the spectra of seismic shear waves from earthquakes. *J. Geophys. Res.*, **75**, 4997-5009.
- Brune, J. and J. Dorman (1963). Seismic waves and earth structure in the Canadian shield, *Bull. Seism. Soc. Am.*, **53**, 167-209.
- Ekström, G. A. and A. M. Dziewonski (1985). Centroid-moment tensor solutions for 35 earthquakes in western North America (1977-1984), *Bull. Seism. Soc. Am.*, **75**, 23-39.

- Greive, R., and Therriault, A. (2000). Vredefort, Sudbury, Chicxulub; three of a kind? *Annual Review of Earth and Planetary Sciences*, **28**, 305-338
- Hanks, T. and H. Kanamori (1979). A moment magnitude scale. *J. Geophys. Res.*, **84**, 2348-2350.
- Kaka, S. and G. Atkinson (2004). Relationships between Instrumental Ground Motion Parameters and Modified Mercalli Intensity in Eastern North America, *Bull. Seism. Soc. Am.*, **94**, 1728-1736.
- Kaka, S. and G. Atkinson (2005). Empirical Ground-Motion Relations for ShakeMap Applications in Southeastern Canada and the Northeastern United States, *Seismological Research Letters*, **76**, 274-282.
- Ma, S. and G. Atkinson (2006). Focal Depths for Small to Moderate Earthquakes ($mN < 2.8$) in Western Quebec, Southern Ontario, and Northern New York. *Bull. Seism. Soc. Am.* **96**, 609-623.
- Mereu, R., D. Wang, O. Kuhn, D. Forsyth, A. Green, P. Morel, G. Buchbinder, D. Crossley, E. Schwarz, R. duBerger, C. Brooks and R. Clowes (1986). The 1982 COCRUST seismic experiment across the Ottawa-Bonnechere graben and Grenville Front in Ontario and Quebec. *Geophys. J.R. Astr. Soc.*, **84**, 491-514.
- Milkereit, B. Green, A. and the Sudbury Working Group. (1992) Deep geometry of the Sudbury structure from seismic reflection profiling. *Geology*, **20**, 807-811.
- Ogata, Y. (1988). Statistical models for earthquake occurrences and residual analysis for point processes. *J. Amer. Stat. Assoc.*, **83**, 9-27.
- Ogata, Y. (1999). Seismicity analysis through point-process modeling: A review. *Pure and Applied Geophysics*, **155**, 471-507.
- Pye, E.G., Naldrett, G.J. and Gibbin, P.E., eds., (1984) The geology and ore deposits of the Sudbury structure. Ontario Geological Survey Special Volume I, 603 pp.
- Randall G. (1994). Efficient calculation of complete differential seismograms for laterally homogeneous earth models, *Geophys. J. Int.* **118**, 245-254.
- Riller, U. (2005). Structural characteristics of the Sudbury impact structure, Canada: Impact-induced versus orogenic deformation—A review. *Meteoritics & Planetary Science*, **40**, 11, 1563-1752.
- Shcherbakov, R., Turcotte, D.L., and Rundle, J.B., 2004. A generalized Omori's law for earthquake aftershock decay. *Geophys. Res. Lett.*, **31**, L11613, doi:10.1029/2004GL019808.
- Siddiqi, J. and G. Atkinson (2002). Ground motion amplification at rock sites across Canada, as determined from the horizontal-to-vertical component ratio. *Bull. Seism. Soc. Am.*, **92**, 877-884.

Table 1 – Distances from SNO stations (and CNSN station SUNO) to the MN4.1 Lively event (at depth 2.35 km).

Station	Horizontal distance	Vertical distance	Hypocentral distance
SUNO	22. km	2.35 km	22. km
SSNO	1.28	2.35	2.7
11SNO	2.31	2.35	3.3
46SNO	0.90	0.94	1.3
LSNO	0.93	0.27	1.0
DSNO	0.34	0.27	0.44

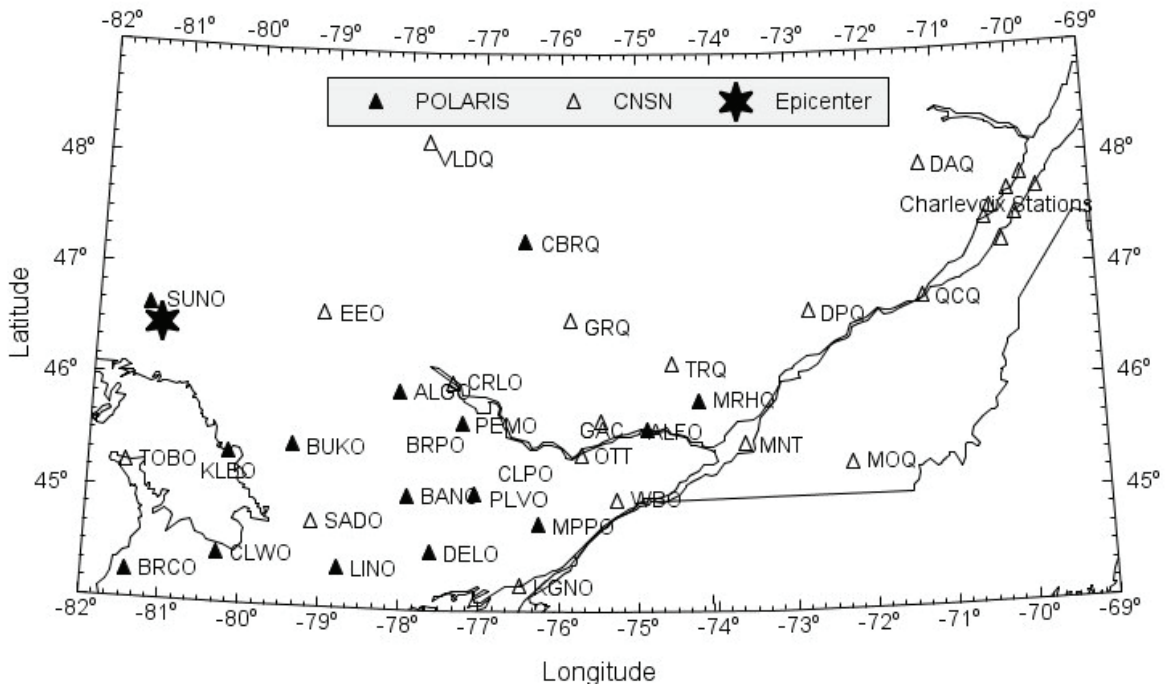


Figure 1 – Location of Lively event (star) and regional seismicographic stations (triangles). Five local SNO stations are located beneath the star.

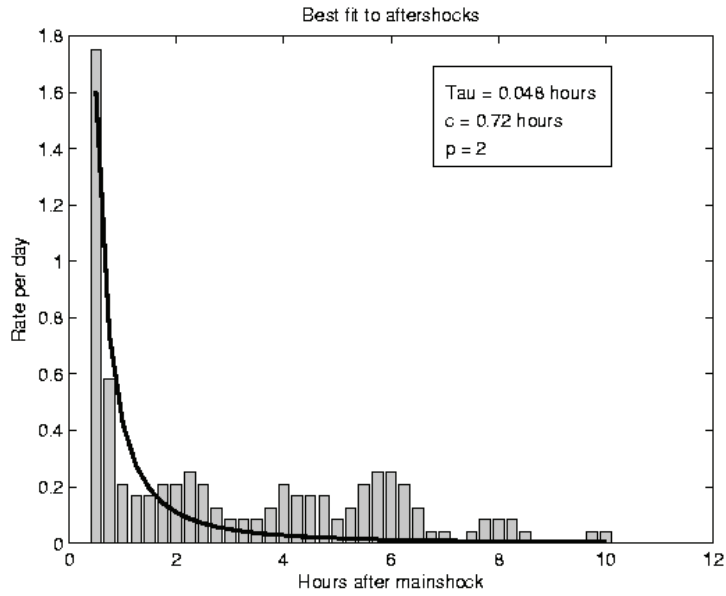


Figure 2 –Decay in rate of aftershock occurrence (bars) computed by counting the number of observed aftershocks within a moving 1-hour time window. Curve shows computed aftershock rate using the modified Omori formula.

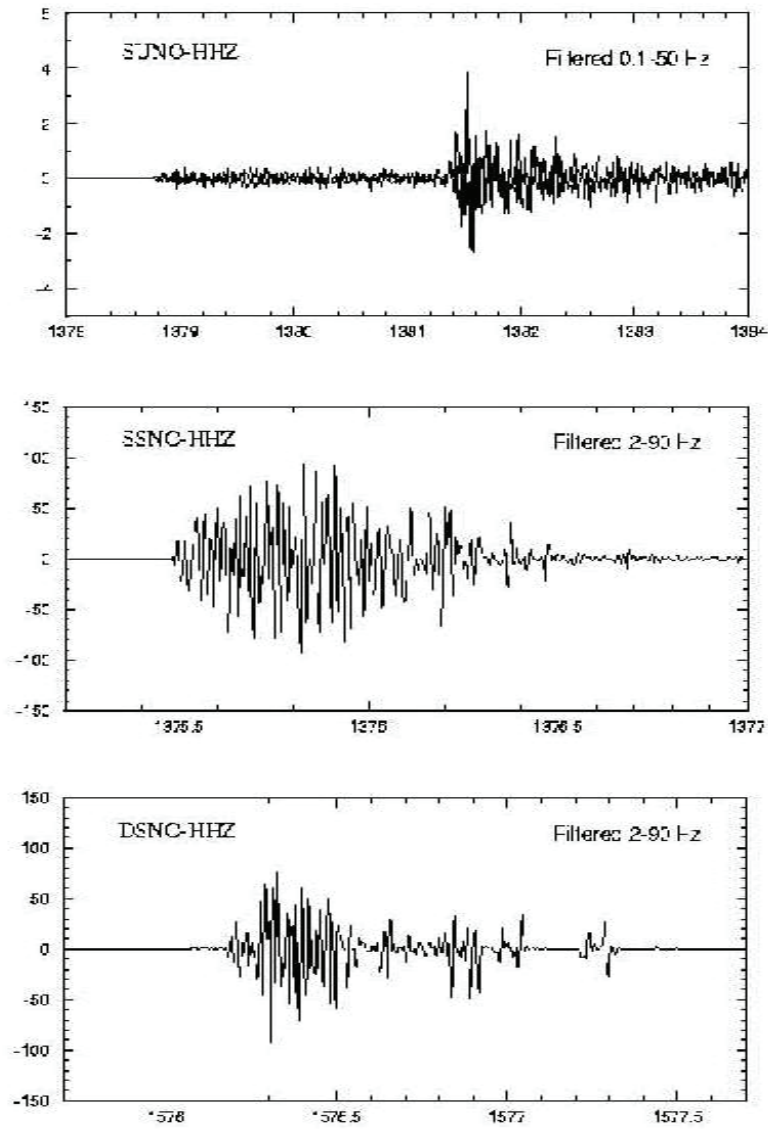
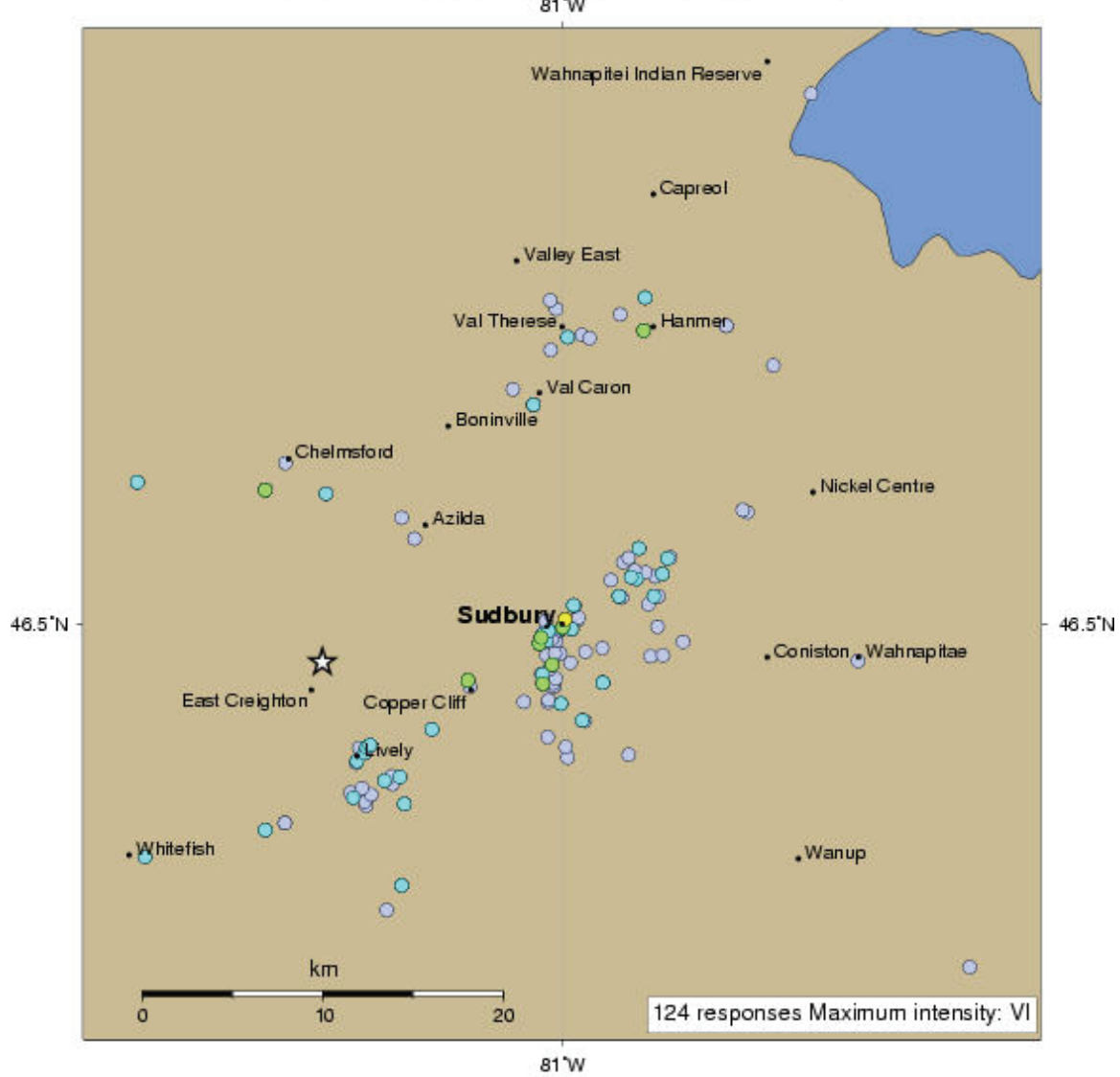


Figure 3 – Velocity records from the Lively event at SUNO ($r = 22$ km), on the surface at SNO (SSNO, $r = 3$ km) and at depth (DSNO, $r = 0.4$ km). Vertical component is shown. Records filtered 5-50 Hz.

GSC Community Internet Intensity Map for Lively, ON event (Nov 29 2006)

02:22:55 EST Mag=4.1 Latitude=N46.48 Longitude=W81.18



INTENSITY	I	II - III	IV	V	VI	VII	VIII	IX	X+
PERCEIVED SHAKING	Not felt	Weak	Light	Moderate	Strong	Very Strong	Severe	Violent	Extreme
POTENTIAL DAMAGE	none	none	none	Very light	Light	Moderate	Moderate/Heavy	Heavy	Very Heavy

Figure 4 – Community internet intensity observations from the Lively earthquake (www.earthquakescanada.ca)

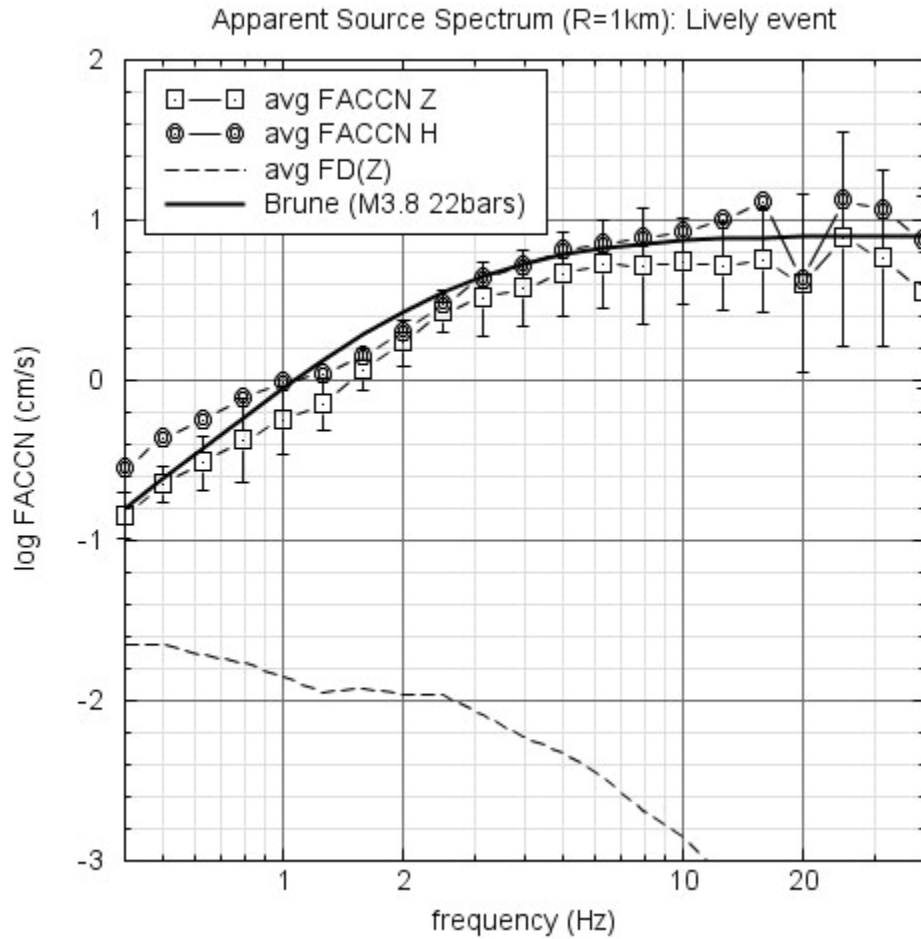


Figure 5 – Apparent source spectrum for Lively event, at $r = 1$ km, based on surface stations on rock. Symbols show mean Fourier acceleration, for vertical and horizontal components; standard deviation shown for vertical component only (variability is similar for horizontal component). Dashed line is Fourier displacement spectrum for the vertical component. Heavy line shows Brune model Fourier acceleration spectrum for M3.8 with 22 bar stress drop.

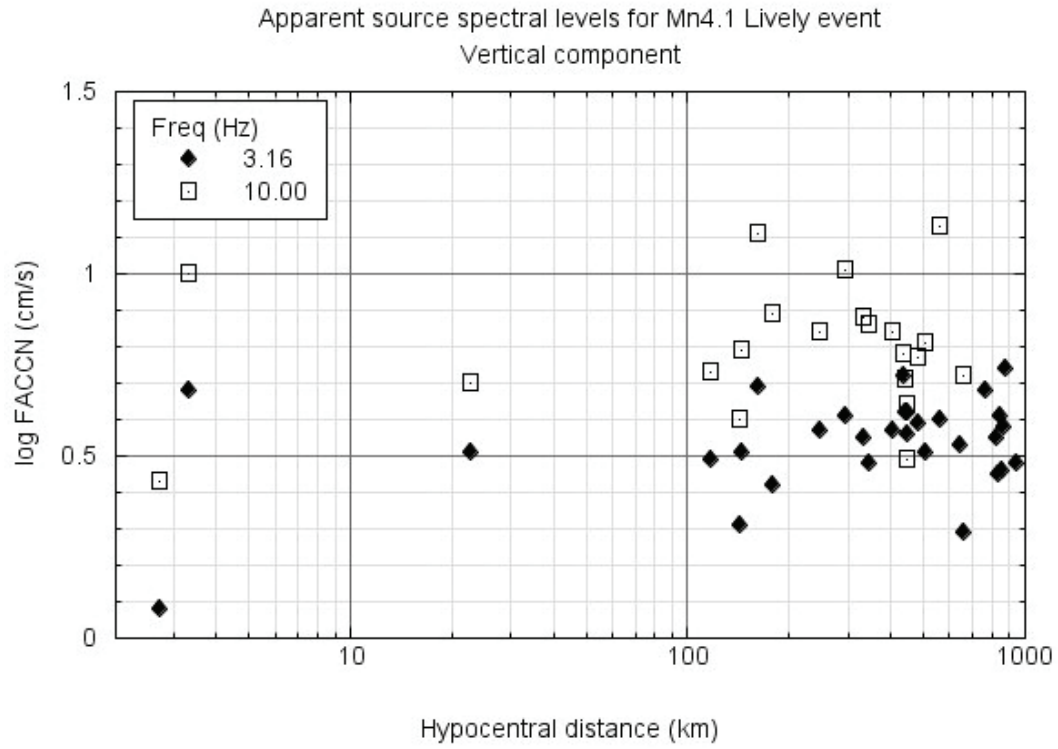
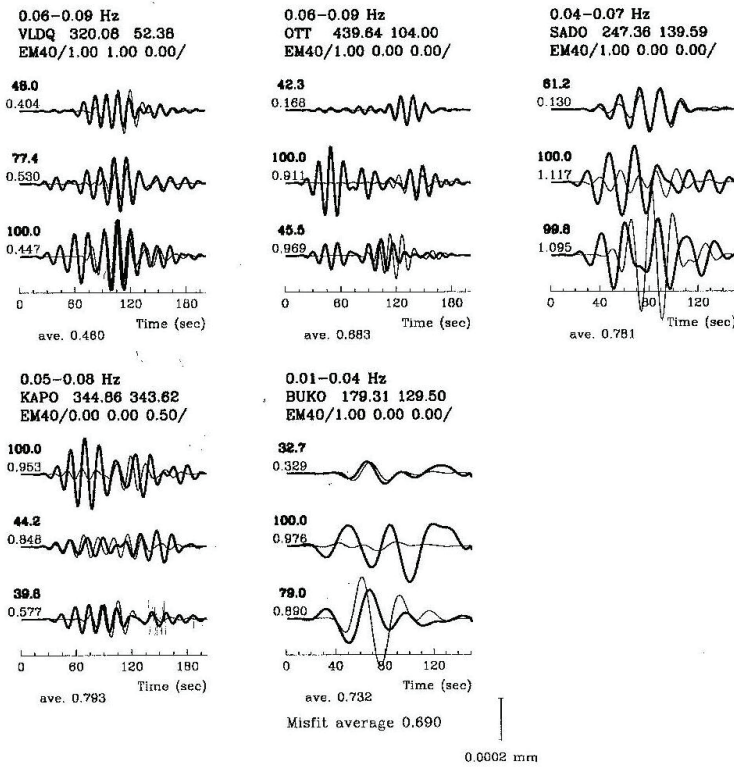


Figure 6 – Apparent source acceleration level for selected frequencies, as a function of distance of the observation from the earthquake source (vertical component). There are no trends with distance.



2006/11/29 7:22:55.1

(46.4822, -81.1675)

Depth = 7 km Mw = 3.71

4.562×10^{21} dyne-cm

Strike Dip Slip

Plane 1: 118.95 63.23 157.85

Plane 2: 219.34 70.33 28.58

CLVD = 32.7%

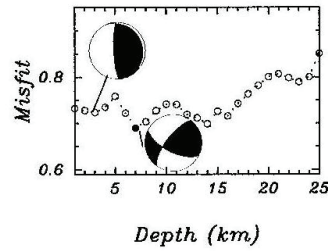
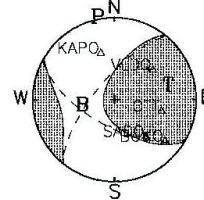


Figure 7 – Moment tensor inversion of Lively event. For each station, the top line gives the frequency range modeled; the second line gives the station code, distance in km and azimuth in degrees; the third gives the velocity model (EM40=Brune and Dorman, 1963 with 40 km thick crust) and the weight given to each component for the inversion. The data and synthetics are plotted for each component - the thicker line is the data. The top number gives the amplitude of the component as a percent of the largest component. The second number is the misfit. On focal mechanism plot, the dashed lines are for the best fit double couple and the shading is for the complete moment tensor solution. In the depth vs. misfit plot the best fitting double couple mechanisms are shown for the preferred depth from the inversion as well as the preferred depth based on very close stations.

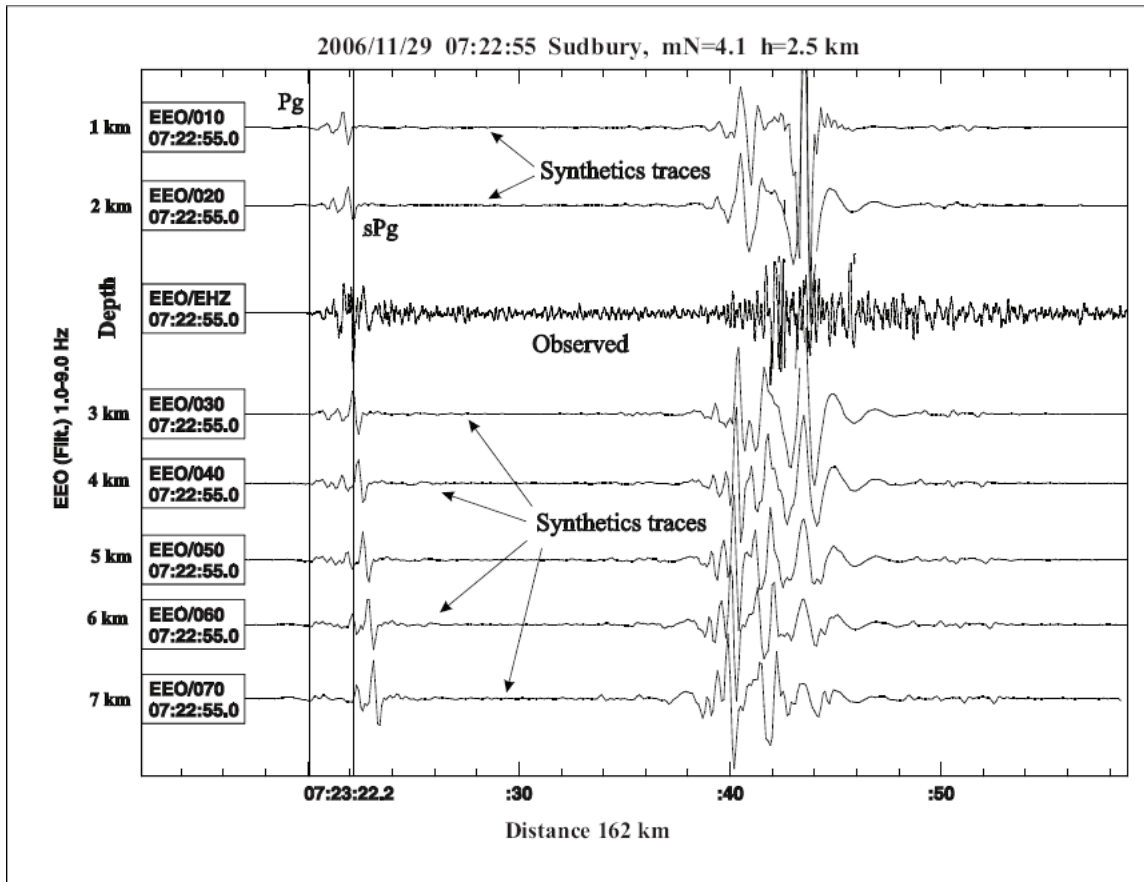


Figure 8 – Regional depth phase modeling at station EEO. The best match of relative arrival times of sPg and Pg, between the synthetics and the data, is obtained for a depth of 2.5 km. Note also the well-developed Rg phase.

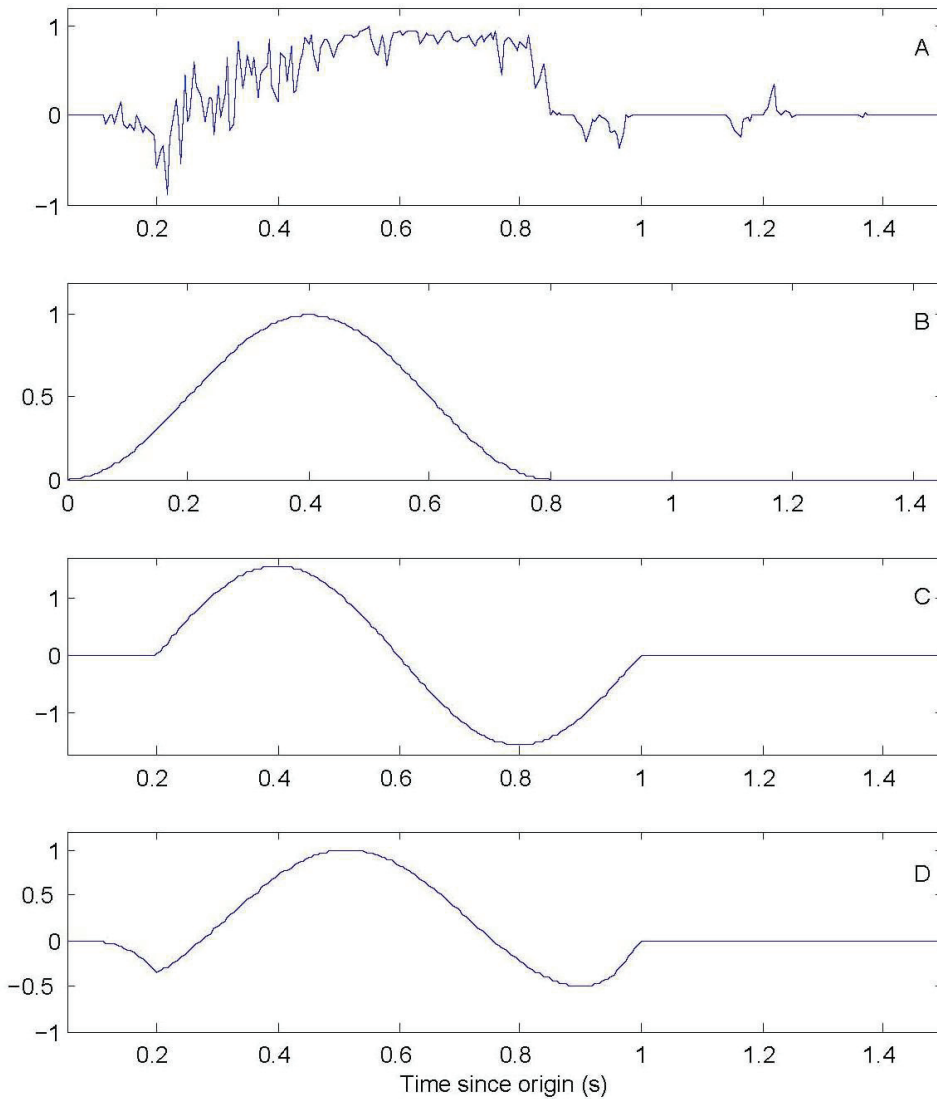


Figure 9 – A) Unfiltered vertical-component recording of the mainshock at station DSNO, 0.4 km from the focus. Note aftershocks at ~ 0.9 and 1.15 s. B) Source time function used to compute synthetic seismograms, with period $T = 0.8$ s. C) Synthetic seismogram computed using the moment tensor determined by regional waveform modeling within only far-field terms. The radiation pattern is dominated by the S-wave, which has a waveform that is the time derivative of the source time function in B. D) Synthetic seismogram computed using the same moment tensor, but with near-source terms included. Interference of the near- and far-field terms reproduces some features of the observed waveform, such as the initial negative ground motion.

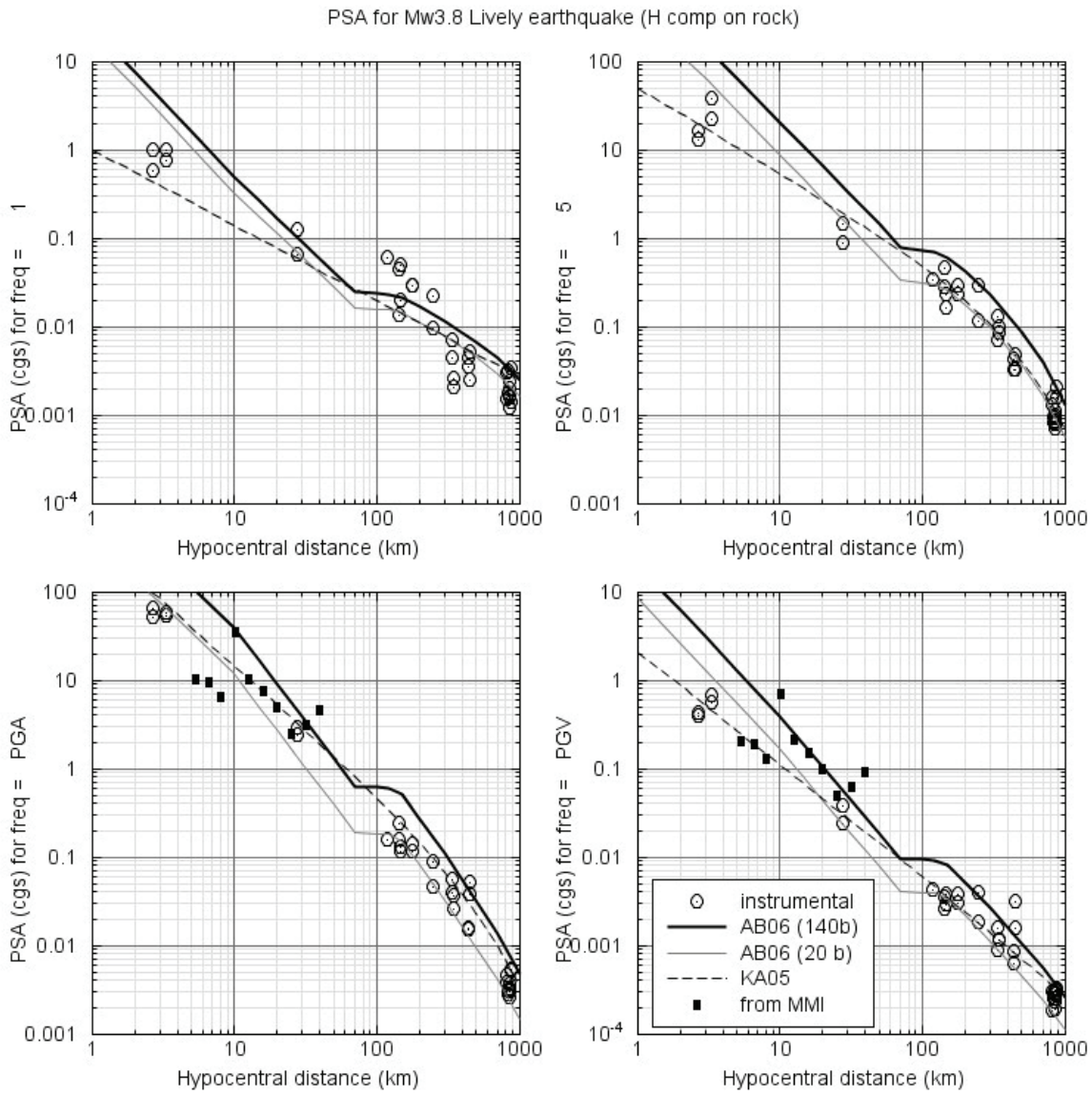
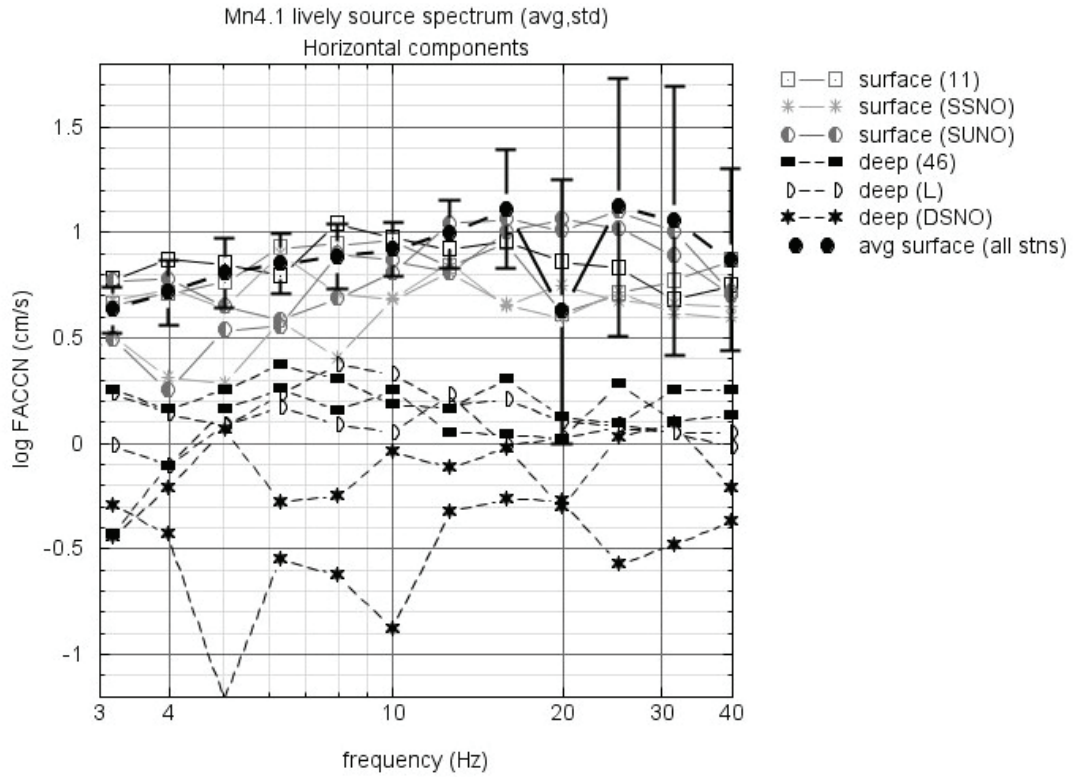
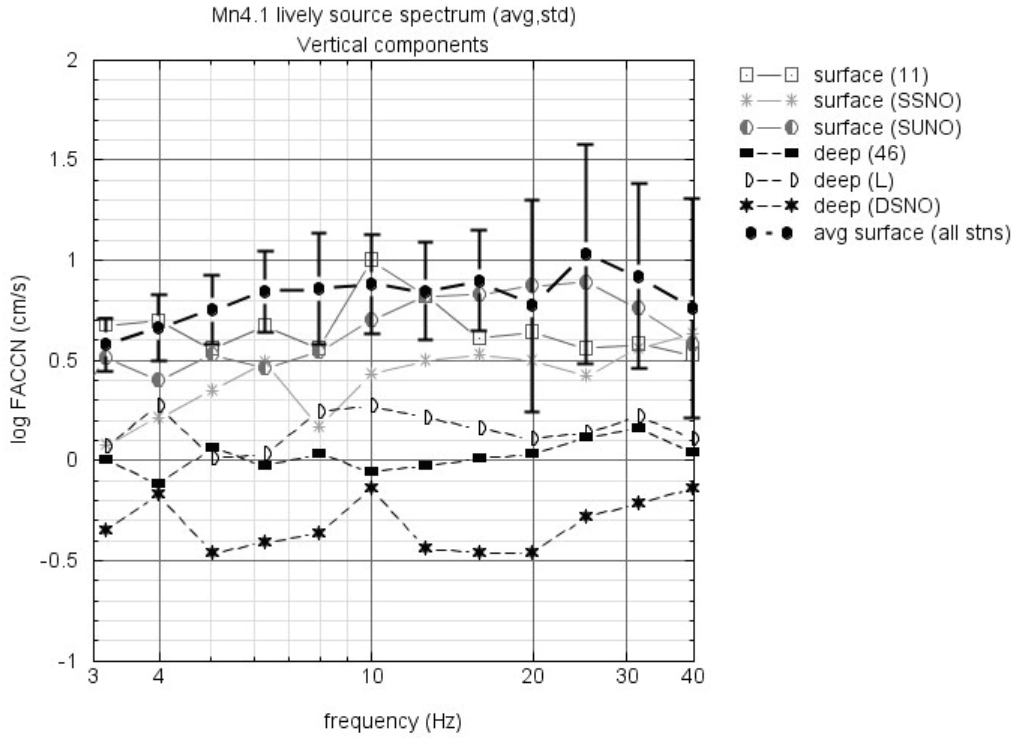


Figure 10 – Observed PSA from the Lively earthquake, in comparison to predictions of the Atkinson and Boore (2006) equations for rock, for stress drops of 140 bars and 20 bars. The empirical prediction equations of Kaka and Atkinson (2005) for ShakeMap applications are also shown. Circles show instrumental data, squares are estimates from MMI.



Subsurface stns not corrected for distance

Figure 11 – Horizontal-component apparent source spectra at the surface, corrected to $r = 1\text{ km}$, are shown by solid lines for stations SSNO and 11SNO (near $r = 3\text{ km}$) and SUNO (near $r = 22\text{ km}$). Apparent source spectrum at $r = 1\text{ km}$ from all stations shown by black symbols (mean and standard deviation). Dotted lines show subsurface spectra, NOT corrected for distance, at 46SNO and LSNO (both near $r = 1\text{ km}$), and at DSNO (at $r = 0.4\text{ km}$).



Subsurface stns not corrected for distance

Figure 12 – Vertical-component apparent source spectra at the surface, corrected to $r = 1\text{ km}$, are shown by solid lines for stations SSNO and 11SNO (near $r = 3\text{ km}$) and SUNO (near $r = 22\text{ km}$). Apparent source spectrum at $r = 1\text{ km}$ from all stations shown by black symbols (mean and standard deviation). Dotted lines show subsurface spectra, NOT corrected for distance, at 46SNO and LSNO (both near $r = 1\text{ km}$), and at DSNO (at $r = 0.4\text{ km}$).